APPENDIX A

Supplemental Declaration of Dr. Max Sonnleitner Under 37 C.F.R. § 1.132

PATENT

IN THE UNITED STATES PATENT AND TRADEMARK OFFICE

In re Application of: Hansgeorg Schindler	Group Art Unit: 1639
Serial No.: 09/845,006	Examiner: Jon D. Epperson
Filed: April 27, 2001	Atty. Dkt. No.: SONN:010US
For: ARRANGEMENT FOR VISUALIZING MOLECULES	

CERTIFICATE OF MAILING
37 C.F.R. § 1.8

I hereby certify that this correspondence is being deposited with the U.S. Postal Service as First Class Mail in an envelope addressed to: Commissioner for Patents, P.O. Box 1450, Alexandria, VA 22313-1450 on the date below.

April 7, 2006 — Mark B. Wilson
Date

SUPPLEMENTAL DECLARATION OF DR. MAX SONNLEITNER UNDER 37 C.F.R. §1.132

Commissioner for Patents
PO Box 1450
Alexandria, VA 22313-1450

I, the undersigned, do declare that:

1. I am Head of the "Ultra-sensitive Fluorescence Microscopy/Device Development" group at the Center for Biomedical Nanotechnology of the Upper Austrian Research GmbH in Linz, Austria. I have over 7 years of research experience and have published numerous peer-reviewed publications in the field of fluorescence microscopy. I am an expert in, among others, the area of fluorescence microscopy, including single molecule detection

and single dye tracing. A copy of my *curriculum vitae*, listing my publications in this regard, was attached to the previous Declaration I submitted in connection with the above-referenced case.

2. I am familiar with the work of Dr. Hansgeorg Schindler relating to single molecule imaging on large surface areas using fluorescence microscopy and a CCD camera synchronized to a sample scanning stage. I have reviewed the specification and currently pending claims in the above-referenced case, in addition to the Official Action dated November 8, 2005 ("the Action"). I am submitting this Supplemental Declaration to provide further support for the statements I made in my previous Declaration of June 16, 2005, which I was asked to provide in the above-referenced case.

3. As I stated in my previous Declaration, the term "large-area fluorescent excitation" as used in the specification and claims has the same meaning to one of skill in the field of fluorescence microscopy as the term "wide-field illumination." Further, one of skill in the field would understand that "large-area fluorescent excitation" is a completely different technique than confocal microscopy. These statements are supported by the following evidence:

- the article "Ultra-Sensitive Fluorescence Reader for Bioanalysis" by Hesse, *et al.*, Cur.Pharma.Biotechnol. 5 (2004):309-319 ("Hesse-1") (attached as Appendix B), which makes frequent reference to illuminating "large sample areas" (p. 310, col. 1) during a process referred to as "wide field illumination" (p. 311, Fig. 1B and description);
- the article "Single-Molecule Reader for Proteomics and Genomics" by Hesse, *et al.*, J. Chromatography B 782 (2002):127-135 ("Hesse-2") (attached as Appendix C), which explicitly differentiates confocal microscopy (p. 128, col. 2) from an approach in which "large sample areas are illuminated" (p. 129, col. 1), a process referred to as "large area screening" (Abstract);

- the article "High-throughput scanning with single molecule sensitivity" by Sonnleitner, *et al.*, Proc. SPIE, 5699 (2005):202-210 ("Sonnleitner-1") (attached as Appendix D), which explicitly differentiates (in Section 2.1) confocal scanning from a scanning technique that involves "large areas," which is referred to as "wide-field illumination"; and

- the fact that the German word "großflächig," which I understand was used in the original, un-translated application in the above-referenced case, may be translated in English as either "large-area" or "wide-field."

4. Given that large-area fluorescent excitation is a completely different technique than confocal microscopy, a light source, such as a laser, is not inherently configured for use in either technique. A light source that is configured for use in confocal microscopy would necessarily be different from a light source that is configured for use in large-area fluorescent excitation.

5. I have read the statement in the Action that the term "large-area fluorescent excitation" is a relative term that is indefinite and/or unclear. I disagree with this statement because a person skilled in the field of fluorescence microscopy would easily understand the meaning and scope of this term. Namely, as set forth above, they would understand that it is synonymous with the term "wide-field illumination."

6. I have read the statement in the Action that the Sharonov and Sanchez references disclose a light source that is adapted for large-area fluorescent excitation. I disagree with this statement because the Sharonov and Sanchez references are directed entirely to confocal microscopy. As set forth above, given the differences in large-area fluorescent excitation and confocal microscopy, a light source that is configured for use in confocal microscopy could not possibly be configured for use in large-area fluorescent excitation. A person

skilled in the field of fluorescence microscopy would understand that Sharonov and Sanchez do not disclose a light source that is configured for use in large-area fluorescent excitation.

7. I hereby declare that all statements made herein of my knowledge are true and that all statements made on information and belief are believed to be true; and further that these statements were made with the knowledge that willful false statements and the like so made are punishable by fine or imprisonment, or both, under Section 1001 of Title 18 of the United States Code and that such willful false statements may jeopardize the validity of the application or any patent issued thereon.

27.02.2006
Date

Max Sonnleitner, Ph.D.

APPENDIX B

"Ultra-Sensitive Fluorescence Reader for Bioanalysis" by Hesse, *et al.*, Cur.Pharma.Biotechnol. 5 (2004):309-319

Ultra-Sensitive Fluorescence Reader for Bioanalysis

Jan Hesse[1], Max Sonnleitner[2] and Gerhard J. Schütz[1,*]

[1]*Biophysics Institute, Johannes-Kepler-University Linz, Altenbergerstr.69, A-4040 Linz, Austria and* [2]*Center for Biomedical Nanotechnology, Upper Austrian Research GmbH, Scharitzerstr.6-8, A-4020 Linz, Austria*

Abstract: Recent advances in the development of new microscopical techniques with single-molecule sensitivity have given access to essentially new types of information on biological systems. In this review, basic methodological concepts of ultra-sensitive microscopy are presented and characterized, with focus on their applicability for a bioanalytical instrument. Measurements on artificial lipid bilayers were used to evaluate the feasibility of this novel technology. First examples of single molecule microscopy on cell membranes revealed new basic insights into the lateral organization of the plasma membrane.

Key Words: single molecule microscopy, scanning device, biochip reader, lipid bilayer, FRET, lateral diffusion, *in vivo*, electrophysiology.

INTRODUCTION

The development of fast fluorescence-based assays in combination with advances in robotics and automization made high throughput screening methods the primary engine driving lead discovery in pharmaceutics. The demand for higher speed in screening techniques drives current methodological developments into two directions: Techniques capable of increased scan rates for a given sample size, and miniaturization of the sample.

The recording-time for a given surface area is defined by the illumination time required to achieve a certain signal-to-noise ratio, the degree of parallelization and additional overheads for exact sample positioning. Highly parallel systems operating at short illumination times with negligible overheads are desired. Illumination times can be reduced easily in cases where a large amount of sample material is available. This requirement is not limiting for the study of model systems, which use cell culture systems. In contrast, only minute amounts of tissue or body fluids are available for routine sample screening. For nucleic acid detection, the problem of limited sample size can be bypassed using PCR-based amplification. Such methods, however, often lead to complications due to cross-contamination of sample material, and distorted statistical outputs. On the contrary, for the analysis of proteins only indirect amplification methods exist [1].

From this line of argumentation, an ultra-sensitive detection device is mandatory for any future genomics and proteomics platform. Steps towards this direction have been taken using gel electrophoresis [2], which allowed quantifying protein expression on single cells. In a different approach, highly sensitive protein-chip read-out has been accomplished using excitation via a planar wave-guide [3]. Recent advances in fluorescence detection techniques extended the range of sensitivity down to the level of single dye molecules [4, 5]. Using such devices, reliable quantification of the number of analytes immobilized on a chip surface is possible at a high dynamic range, from ~10^6 molecules down to 1 molecule per 100μm^2. In order to make such detection devices applicable for diagnostic purposes, high throughput capability has to be ensured. Scanning speeds up to 1cm^2 within ~15 minutes are feasible with current detectors.

INSTRUMENTATION

Pioneering work for the detection and characterization of single fluorescent molecules was performed in the early nineties by several groups, which studied the spectroscopic behavior of single chromophores embedded in condensed matter at low temperature [5, 6]. These studies pushed the limits of sensitivity, however, the systems investigated were far from being biologically relevant. Milestones on the way to applicability in bioscience were reached during the last decade, including single molecule detection at room temperature [7], in buffer [8-10], and in living cells [11-13].

Currently, two strategies are followed for establishing high throughput screening devices at single molecule sensitivity: first, fluorescent molecules in solution are detected by a stationary excitation and detection system. Most prominently, confocal devices have been applied to restrict the detection volume down to a few femtoliters [14]. Using avalanche photodiodes as detectors allows studying the fluorescence intensity, fluorophore transition rates and spatial mobility. Combination of multiple detectors gains additional information about spectral properties. Such devices have been extensively used to study binding kinetics [15], conformational fluctuations [16], spectroscopic transitions [17, 18] and molecular mobilities [19] using fluorescence correlation spectroscopy (FCS, for a review see [20]). This information can be assessed within a few seconds, rendering FCS a promising tool for miniaturized high throughput screening [21]. Fluorescent molecules in

*Address correspondence to this author at the Biophysics Institute, Johannes Kepler University Linz, Altenbergerstr.69, A-4040 Linz, Austria; Tel: +43-732-2468-9284; Fax: +43-732-2468-9280;
E-mail: gerhard.schuetz@jku.at

1389-2010/04 $45.00+.00

solution have been directly imaged on a camera, as they were passing through the defocused excitation beam. The largely increased observation area, compared to a point detector as used for FCS, highly increases detection speed, which has been utilized for DNA fragment sizing [22]. Constant flow of the solution and hydrodynamic focusing ensure that most molecules will pass the detection volume, making this method applicable for detection of trace amounts of analyte molecules.

Second, surface-immobilized molecules can be detected using screening stages. For this purpose, distinct areas of a glass surface are functionalized with capture agents, e.g. antibodies, specific ligands, or cDNA. This procedure allows for parallel investigation of a large number of different fluorescence labeled target molecules on one chip. The basis for ultra-sensitive chip read-out are techniques for detecting single molecules on surfaces. In first studies, confocal microscopy was used to efficiently discriminate single molecule signals from background. The method is based on scanning a diffraction limited laser focus over the sample; the fluorescence emitted from the sample is imaged via a pinhole onto a point detector [23, 24]. Using Avalanche Photodiodes (APD) as detectors allows obtaining additional information about the excited state lifetime. Combination of several APDs placed after a stack of dichroic and polarization beam splitters was used to maximize the information content acquired from a single molecule [17]. However, due to the serial data acquisition the inspection of large sample areas remains a time-consuming task. The time T required for recording an area A at a resolution δ and an illumination time t_{ill} can be estimated by $T = \frac{A}{\delta^2} t_{ill}$. For δ=200nm and t_{ill}=10ms, the time for recording an area A=1cm^2 in a confocal setup is equal to $2.5 \cdot 10^7 s$ (corresponding to 9.3 months).

In a different approach, several groups utilized intensified or back-illuminated CCD-cameras for imaging single molecules on surfaces [8-10, 25-27]. Large sample areas are illuminated with a defocused laser spot and directly imaged. This simultaneous observation was the methodological prerequisite for tracking individual molecules moving in planar systems. In screening assays, parallel observation of many pixels dramatically reduces the recording time T, compared to confocal methods. The time T required for recording a given sample area A can be calculated according to

$$T = \frac{A}{\delta^2} \cdot \left[t_{read-out} + \frac{t_{line-shift}}{C} + \frac{t_{ill} + t_{positioning}}{L \cdot C} \right]$$

The sum represents contributions of the illumination time t_{ill}, the time to digitize each pixel ($t_{read-out}$), the time to shift one line into the read-out register ($t_{line-shift}$) and additional terms accounting for positioning the stage, subsumed in $t_{positioning}$; L and C give the total number of lines and columns on the chip. Frame-transfer cameras acquire signals during the read-out process, which allows neglecting t_{ill}. However, proper sample positioning still limits the overall read-out speed. There, inertia of the moving parts requires time-consuming feedback loops for precise stops. For example, sample shift by 20μm with a precision according to the pixel size of 200nm in the object plane takes about 2s. Assuming a digitization rate of 1MHz, $t_{line-shift}$=12μs, and a chip-size of 1000x1000pixels, an area of 1cm^2 can now be imaged within ~125min.

The principal advantage of using pixel arrays as detectors is parallel signal acquisition. Still, the pixel array covers only a small part of the sample area A, making additional scanning of the sample inevitable. A proper way for reducing overhead times due to stage positioning and signal integration is the implementation of synchronized continuous stage-shift and camera read-out (H. Schindler, international patent PCT/AT9900257). It is based on the Time Delay and Integration (TDI) mode, and allows to decrease the recording time to $T = \frac{A}{\delta^2 N} \cdot \left[N \cdot t_{read-out} + L \cdot t_{line-shift} \right] \approx 1000 s$, corresponding to 42 minutes. In the direction of scanning, the intensity profile of the excitation beam needs not to be constant. In practice, it is convenient to use a Gaussian profile with a width of $\omega \approx L\delta/2$. This ensures maximum excitation of dye molecules within the region of observation, and at the same time minimum photobleaching of dyes in regions still to be scanned.

If the fluorescence intensity, F, would scale linearly with illumination intensity, I, i.e. $F \propto I \cdot t_{ill}$, confocal scanning microscopy could be performed at the same speed as camera-based systems. In this linear regime, focussing of the laser spot by a factor N yields an increased excitation intensity $N \cdot I$, which allows to reduce t_{ill} by a factor N for constant fluorescence emission. However, for high speed single molecule detection it is favorable to operate at illumination intensities close to the saturation intensity of the fluorophore I_S, which is defined by $F \propto (1 + I_S/I)^{-1} \cdot t_{ill}$ [28]. In this case, increase of the intensity has minor effects on F, therefore the illumination time may not be reduced in order to ensure constant signal. Evidently, non-linear effects make camera-based detection systems preferential for ultra-sensitive high throughput screening.

For a discussion of its optical properties, a single dye molecule can be considered as a point light source (Fig. **(1A)**). Its image is characterized by the point-spread function, which describes the spatial distribution of the signal after the imaging process. In the diffraction limit, the in-focus image of a point light source can be approximated by an Airy disk of radius $\rho = 0.61 \times \lambda / NA$, with λ the wavelength of light, and NA the numerical aperture [29]. The non-zero width of the Airy-disk represents the basic limitation to the resolving power of the apparatus used. As a consequence, two point light sources with a distance smaller than ρ cannot be resolved as individual objects. This theorem, known as the "Rayleigh-Criterion", is generally used to define resolution in light microscopy.

In general, the resolution of single molecule microscopy is equivalent to values obtained in conventional fluorescence microscopy, when defined according to the Rayleigh criterion. In other words, the distance r between two molecules of the same fluorophore cannot be determined for $r < \rho$. It is possible, however, to determine the position of

one molecule within the sample with an accuracy of $\Delta r \cong 40nm$ [30-33]; for long illumination times of 0.5s, accuracy values of down to 1.5nm have been reported recently [34]. For unambiguous single molecule probing, the concentration has to be much less than $1/\delta^2$ to ensure that the signals of two molecules do not overlap. Assuming equal distribution of molecules on a surface, the probability that the distance to the nearest neighbor is larger than the size of the diffraction limited spot of r=500nm is given by $F_{nn}(r) = \exp(-r^2 \pi n)$ [35], with n the concentration of dye molecules. For a certainty F>95%, n has to be less than 1molecule/15μm^2.

In order to achieve single molecule sensitivity, the transmission efficiencies of all optical elements in the detection path have to be maximized. In general, the overall detection efficiency, η, can be separated into three factors: the efficiency of the microscope objective, η_O, of optical filters, η_F, and of the detector, η_D. Typical values are: η_O~30% for an oil immersion objective with NA=1.4, η_F~50%, η_D~80%, yielding η~12%. Obviously, the limiting factor is the objective, which collects only a minor fraction of all emitted photons due to the limited collection angle set by the numerical aperture. At optimized settings, such systems allow to obtain images of single dye molecules in synthetic environments at a high signal to background ratio of ~50. Besides high detection efficiencies, this is mainly related to the low noise characteristics of cooled CCD cameras.

Fig. (**1B**) shows a schematic view of the apparatus developed in our lab: Laser light is coupled into an epi-fluorescence microscope, and the emitted light is detected after appropriate filtering on the pixel array of a CCD camera. The excitation beam is defocused to match the region of observation defined by the size of the CCD-array and the chosen magnification of the objective. A homogenous beam profile perpendicular to the scanning direction is achieved using an aspherical lens as beam shaper. For optimum resolution, the step-size of the high precision scanning stage has to fit the pixel size in the image plane, δ. In addition, an autofocus system was introduced to correct for thickness-variations or tilts of the supporting chip-surface. It is based on rapidly refocusing the microscope objective during the scan process. Distance changes of the glass surface from the objective are measured using a second laser at a different wavelength focused onto the chip surface. Angular changes of the back-reflected beam are detected on a two-segment photodiode and corrected by shifting the objective [36].

INFORMATION CONTAINED IN SINGLE MOLECULE IMAGES

The fluorescence image of a dye molecule contains two parameter accessible by a camera as a detector: first, the

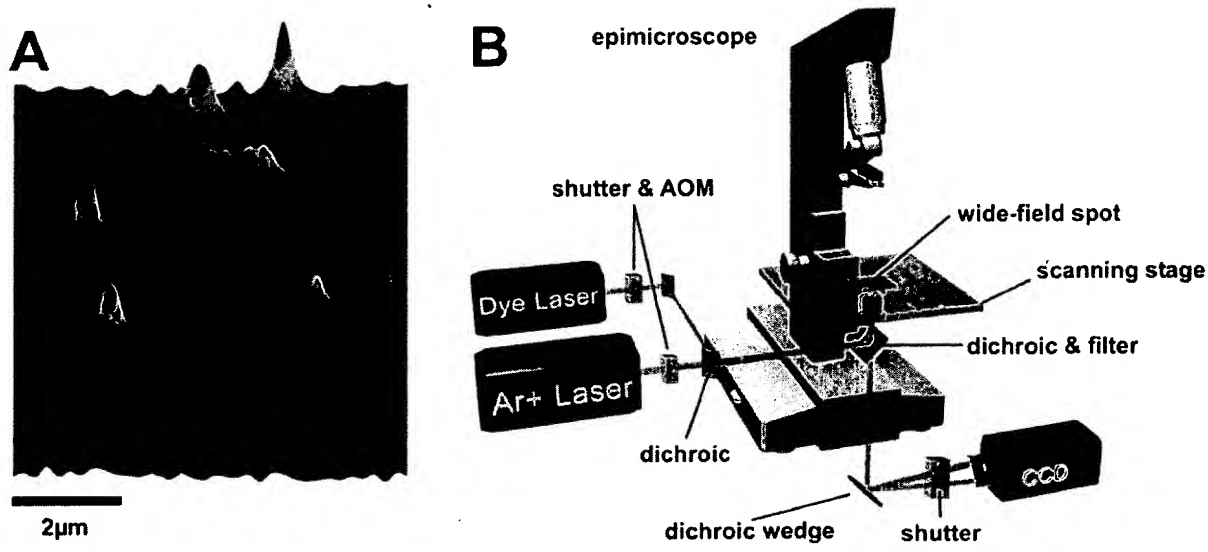

Fig. (1). A) Fluorescence image of single Cy5-labelled thy1 molecules on a human aorta smooth muscle (HASM) cell. Using image processing algorithms, it is possible to locate and quantify single-fluorophores with a positional accuracy of ~40nm. **B)** Schematic overview of the microscope. Laser light from an Ar^+-Laser (514nm) and a dye-Laser (633nm) is combined to a single beam using a dichroic beamsplitter. Electronic shutter elements and Acousto-Optical-Modulators (AOMs) allow for precise control of illumination times. Excitation of the target molecules in the sample takes place in a spot of approximately 20µm in diameter ("wide field illumination"). This beam geometry is achieved by placing a defocusing lens between the lasers and the objective. Emitted fluorescence light originating from the sample is collected via an oil immersion objective (100x, NA=1.4), and, after appropriate filters, reflected by a dichroic wedge. Light with λ<650nm is reflected from the front surface of the wedge ("green" channel), whereas light with λ<660nm is reflected from the rear surface ("red" channel). The tilt angle of ~1° between front and rear surface leads to two separate images on the CCD camera – one for each spectral region – with a distance of ~100µm on the chip. For scanning purpose, the laser beam is shaped by an aspherical lens to the desired line-profile, and projected onto the sample. A high precision scanning stage is synchronized with the read-out of the camera, operated in TDI mode.

position of the molecule, which is given by the center of its signal. This can be determined to an accuracy much below the wavelength of light; ~40nm can be achieved routinely for positioning single biomolecules at room temperature using wide field microscopy [33]. Second, its *fluorescence intensity*, which can be quantified by the number of photons detected from the molecule during the illumination time. This number can be taken as a characteristic property of the dye molecule under constant environmental conditions. A third parameter, the *fluorescence lifetime*, is only measurable using point detectors or gateable intensified cameras [37]; for a critical discussion of the implications of lifetime analysis for single molecule studies we refer to [5] and [17]. In the following, several aspects of single molecule studies based on these observables will be highlighted.

Local Stoichiometry

In general, a single dye molecule emits a well-defined number of photons during a given illumination time, which is a characteristic parameter of the molecule. The fluorescence signal obtained from a single biomolecule can thus be used as a measure for the number of bound fluorophores. This principle has been employed in rather different fields like sizing of fluorescently stained DNA-fragments [38, 39], as well as molecular counting of low-density lipoprotein particles on cell surfaces [40]. The critical point in all methodologies utilizing fluorescence intensity for sizing is the reliability of the assignment. Using randomly labeled particles, the accuracy of discrimination between n and n+1 associated particles scales with $\sqrt{N}$, with N the mean number of fluorophores per particle. Therefore, high discrimination accuracy requires heavily labeled particles.

In the single fluorophore regime, reliable stoichiometric assignment is possible by using labeling at a defined ratio. The reliability then depends only on the inherent intensity fluctuations of the dye molecule used. In this regime of very low fluorescence intensities, the stochastic nature of photon emission leads to statistical distributions of the actually detected fluorescence. Those distributions can be characterized and taken into account for probabilistic assignment of local stoichiometries. Using the approach of single molecule counting, the number of fluorescence labeled ligands bound to individual membrane anchored receptor molecules could be determined, allowing for digital analyte quantization on a molecular level [41].

Co-Localization of Different Molecules

Two different strategies have been employed to study colocalization of different molecules: single pair Fluorescence Resonance Energy Transfer (FRET) [42] and dual wavelength imaging [43]. FRET between donor and acceptor dyes, also termed Förster energy transfer [44], is, in application to ensembles, a well-established assay for the study of colocalization or clustering of components in, for example, cell membranes [45-47]. Recently, FRET was carried to the ultimate limit of the energy transfer between a single pair (donor-acceptor) of biomolecules (single pair FRET; for a review see [48]). The strong distance dependence between donor and acceptor molecule on length scales of ~5nm was utilized to quantify distances on single DNA molecules [42, 49], to observe conformational dynamics on single enzymes [50], and to image ligand colocalization on individual receptor molecules [51]. Even first applications to living cells have been demonstrated recently [11].

Dual wavelength imaging, the alternative approach to colocalization, visualizes the positions of two different dye molecules in the same probe. The two images are acquired either consecutively [51] or simultaneously [43, 52-54] by imaging the same sample area containing two different dyes using two spectroscopic channels specific for the two fluorophores.

Orientation

Light absorption of a fluorophore depends on the angle between the polarization of the excitation light and the orientation of the transition dipole of the dye. Using linear polarized light for excitation allows determining the orientation of a single fluorescent dye by measuring the modulation of the fluorescence signal [55-58]. This is equivalent to measuring the linear dichroism of a single dye. In addition, the polarization of the fluorescence signal emitted from the fluorophore can be determined by introducing a polarizing beam-splitter into the emission path of the microscope [59-61]. This methodology has been applied for determination of the axial rotation of actin filaments sliding along myosin molecules [59], for monitoring conformational changes in single myosin molecules [60], and for observation of the rotational diffusion of individual lipids in an artificial lipid membrane [61] (see also below). Combination of both polarized excitation and determination of the emission polarization allows for steady-state anisotropy measurements on a single molecule [61, 62], which opens up the possibility to access nanosecond time-scales for probing single molecule reorientation. This technique does not interfere with simultaneous determination of the lateral mobility of the same molecule, which allows to correlate the rotational diffusion of a single lipid molecule measured on a ns time scale with the lateral mobility on a ms time-scale [61]. In addition, determination of the polarization can be performed for two colors simultaneously [17, 53]. This allows combined measurements of dye orientation and energy transfer, yielding much deeper insights into molecular reorganizations of large biomolecules.

The basic limitation of this approach is its restriction to the study of the in-plane component of the orientation of a dye molecule. In conventional wide-field microscopy, the polarization of the excitation light lies mainly within the focal plane. Attempts to access the full orientation of a molecule are therefore based on methodologies with a strong z-component in the polarization, like near field microscopy [63, 64] or modified confocal microscopy [65]. From the image pattern, the azimuth and elongation angle of a dye molecule can be calculated.

SINGLE MOLECULE DYNAMICS IN ARTIFICIAL SYSTEMS

From the beginning of cell biology, biomembranes were considered to be of major relevance for cellular function.

Each cell is separated from its environment via a biomembrane. Biomembranes enable the division of the cell cytoplasm into chemically distinct subspaces, thereby governing the development of cell organelles. Moreover, biomembranes act as hosts for integral, lipid-anchored or adsorbed membrane proteins, and thereby considerably affect protein function.

The role of lipids as the major constituents of biomembranes has been established in the seventies, leading to the proposition of the fluid mosaic model for cell membranes [66]. In this model, it was the lipids and not the proteins that were assumed to constitute the matrix of the cell membrane. Since this matrix was shown to be in a fluid state, integral membrane proteins were expected to be free to diffuse laterally within the membrane, as long as no interaction with cytoskeletal elements hinders their Brownian motion.

The choice of the right testing system is one crucial factor when establishing a novel methodology. From the beginning, it was clear in our lab that one area of application should be mobility measurements on biomembranes. While the native plasma membrane represents the more relevant system, artificial bilayers are advantageous as a test bed since they can be prepared at a level of highest-grade purity. No fluorescence signal was observable from a pure palmitoyl-oleyl-phosphocholine (POPC) bilayer, while mixing POPC with increasing amounts of a fluorescent lipid analogue (N-(6-tetramethylrhodaminethiocarbamoyl)-1,2-dihexadecanoyl-sn-glycero-3-phosphoethanolamine, TMR-DHPE) resulted in an increased fluorescence intensity detected from the membrane [10, 28]: at high molar ratios of labeled lipid, a homogenous signal was detected, whereas at lower concentrations, individual peaks could be resolved, which were moving within the membrane. It was suggestive to ascribe those peaks to single TMR-DHPE molecules diffusing in the bilayer. They were observed to photobleach in a one-step manner, a common criterion for single molecule observation. To unambiguously prove single molecule observation, however, consistency with ensemble measurements had to be checked. For this, we measured the average fluorescence signal per pixel at various molar ratios of fluorescent lipid analogue; a strictly linear relationship was found. Together with the known mean area of a single lipid of A=63Å^2 [67], the signal value of a single dye molecule could be predicted, which showed perfect agreement with the signal obtained from individual peaks at low concentration. Finally, the signal values were also consistent with theoretical predictions drawn from photophysical calculations.

Having certainty about the origin of the observed fluorescent peaks being single lipid molecules, applications of this novel device to membrane biology have been faced. In a first approach, the mobility of individual lipid molecules within the membrane was measured by studying the mean-square displacement, r^2, as a function of the time lag between two observations of the same molecule, t_{lag}. As expected for free Brownian motion, the data followed a linear relationship according to $r^2 = 4Dt_{lag}$ [10]. No indication for any deviation from free diffusion could be inferred from this analysis. Unfortunately, methods developed for more detailed analysis of trajectories recorded in single particle tracking experiments [68-71] were not applicable here due to the comparatively short length of single molecule trajectories. Therefore, we introduced a novel type of analysis, based on the statistical examination of the measured displacement values [33].

The probability that a molecule will be found within a distance r from its starting point at time t_{lag} is, assuming Brownian motion, given by

$$P\left(r^2, t_{lag}\right) = 1 - \exp\left(-r^2 / r_0^2\right)$$

The characteristic decay constant, r_0, is given by $r_0^2 = 4Dt_{lag}$. According to this model, a mono-exponential increase of P as a function of r^2 would be expected. Interestingly, clear deviations from a mono-exponential function have been observed for the diffusion of TMR-DHPE in a POPC bilayer. Closer inspection of the data revealed two distinct types of mobility with decay constants r_1^2, r_2^2, following

$$P\left(r^2, t_{lag}\right) = 1 - \left[\alpha \cdot \exp\left(-r^2 / r_1^2\right) + (1-\alpha) \cdot \exp\left(-r^2 / r_2^2\right)\right]$$

In this bi-exponential model, α denotes the fraction of the molecules showing decay constant r_1. While 75% of the observed displacement steps belong to a rapid diffusion (D_1=4.4μm^2/s), 25% correspond to molecules that were nearly immobilized (D_2=0.07μm^2/s). This fraction has to be compared to the immobile fraction in photobleaching experiments, which was found to be in a range of up to 25% [72, 73]. This partial immobilization of lipids was speculated to be caused by interactions between the support and the bilayer.

In order to further address this point, we fabricated a measurement chamber, which allows the investigation of free-standing bilayers using the same SDT instrument [74]. In this chamber, a black lipid membrane was painted over an 80μm hole within a thin Teflon sheet, located 150μm above the glass slide. For microscopy, the oil immersion objective was replaced by a high NA water objective with a considerably longer working distance. Individual Cy5-DHPE molecules were easily identified within the black lipid membrane, and the same type of analysis was applied. For the freestanding bilayer, no deviations from the mono-exponential probability distribution have been detected. In contrast to the supported membrane, the mobility of individual lipids within a black lipid membrane was found to be pure diffusion. This finding further indicates a massive effect of the glass slide onto the mobility of supported lipid bilayers.

Lateral diffusion can be microscopically detected over length scales of δr~40nm, corresponding to millisecond time scales. Rotational diffusion in fluid bilayers, however, occurs on nanoseconds time scales [75-77] and cannot be assessed directly in a single molecule experiment. Fluorescence anisotropy due to the lipid rotation during the excited state lifetime of the dye molecule enables the indirect

measurement of lipid rotation. To measure single molecule anisotropy, supported lipid bilayers containing trace amounts of fluorescent lipids were illuminated with linear polarized light [61]. The emitted fluorescence signal was splitted in two distinct channels of orthogonal polarization by using a Wollaston prism polarizer. Both channels were imaged on the same CCD camera chip and recorded simultaneously, yielding both the p- (I_P) and s-polarized component (I_S) of the signal. The value of the anisotropy, r, was obtained for each molecule according to $r = \frac{I_P - I_S}{I_P + I_S}$. An average rotational diffusion constant for TMR-labeled lipids of $D_{rot} = 7 \cdot 10^7 rad^2/s$ has been obtained. It should be emphasized that single molecule techniques allow for the simultaneous measurement of rotational and lateral diffusion and their direct correlation, thereby covering six orders of magnitude in time.

Anisotropy allows the indirect measurement of rotational diffusion on a time scale comparable to the excited state lifetime of the fluorophore. In contrast, mobility within bilayers in the gel state are much slower, and can be directly observed by measuring the orientation of the absorption [58] or emission dipole [61] of the dye molecule as it rotates. In analogy to lateral diffusion, the mean square angular displacement $\langle \Delta\Phi^2 \rangle$ increases linearly with time, according to $\langle \Delta\Phi^2 \rangle = 2 D_{rot} t_{lag}$, with the rotational diffusion constant $D_{rot} = 1.2 rad^2/s$. Such experiments represent the methodological pre-requisite for observing structural rearrangements of more complex biomolecules such as site-specifically tagged proteins.

FRET is one of the most sensitive tools for measuring conformational changes of proteins. Site-specific labeling of two distinct protein subunits with two fluorophores enables the detection of rearrangements of those subunits. Since it is possible to measure the molecule *in vivo*, its function may be probed simultaneously. Protein function can be assessed e.g. by measuring the ion-current flowing through the pore of an ion channel, either via patch clamp [78] or via reconstitution techniques [79]. For the *Shaker* potassium channel, distances between the S4-subunits have been measured via FRET at different gating states [80, 81]. In those experiments, specific preparation of all molecules in a distinct gating state was possible by membrane depolarization. In general, however, such synchronization is not feasible due to the lack of determinants for transitions between functional states. In such cases, single molecule methods appear to be the appropriate choice for unraveling the structural origin of a functional change.

From a technical point of view, a modification of an ultra-sensitive microscope, which facilitates simultaneous electrical measurements, seemed straightforward. In our group, a chamber developed for single molecule measurements on black lipid membranes [74] was modified to enable simultaneous electrical measurements [82]. For showing the feasibility of combined electrical and optical measurements on a single molecule level, we decided to measure the pore formation due to the dimerization of two fluorescent gramicidin molecules. Gramicidin is a peptide, which easily incorporates into one leaflet of the lipid membrane. Upon encounter of two molecules in opposing leaflets, a stable pore is formed across the membrane with a lifetime ranging from milliseconds up to seconds [83]. In this model system for an ion channel, two *functional* states can be distinguished: *on* describes an open pore, while *off* is characterized by the absence of any pore within the bilayer; both states can be easily probed electrically. For probing the dimerization process optically, two fluorescent analogues of gramicidin were synthesized by labeling the peptide either with Cy3 or Cy5. With this approach, a *structural* transition

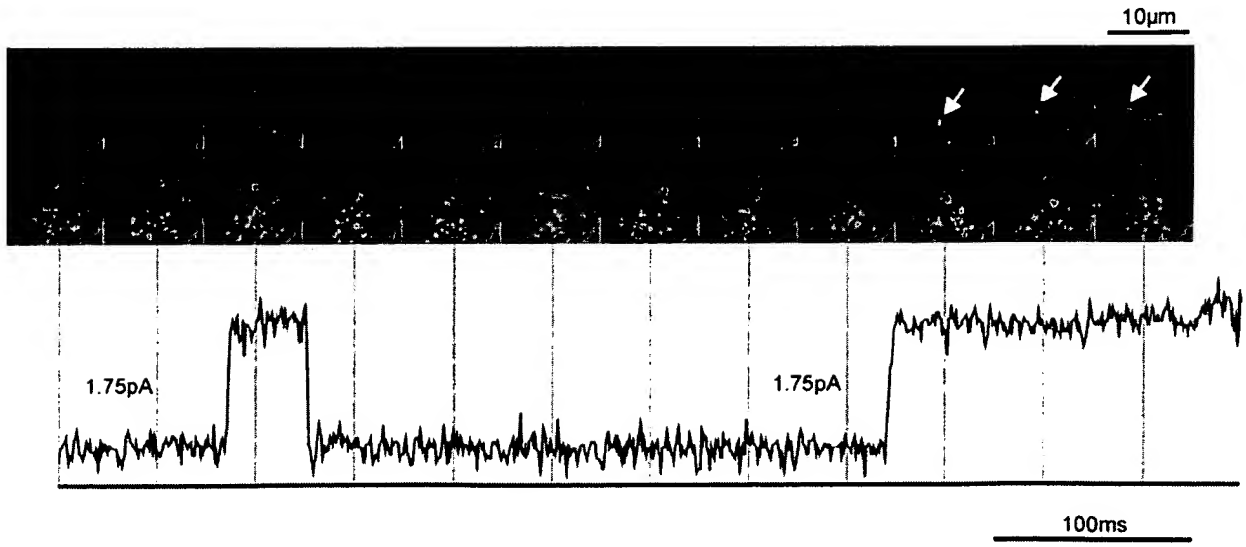

Fig. (2). Fluorescence images (top: Cy5-channel, bottom: Cy3-channel) of a black lipid membrane containing sufficient Gramicidin-Cy3 and Gramicidin-Cy5 to result in single channel openings. FRET events can be observed as bright dots in the red channel (indicated with arrows). Simultaneous electrical recording from the same membrane is shown below. Vertical lines indicate the position of each image in the time record. Reprinted by permission from Biophys.J., [82], copyright 2003 by the Biophysical Society.

from the *monomeric* to the *dimeric* state can be observed via the appearance of a FRET signal. Fig. (2) shows the correlation of such *structural* and *functional* transitions. In the upper panel, the time course of the optical signal of both donor (green) and acceptor (red) is plotted, while the lower panel shows the simultaneously recorded current trace. The formation of two pores can easily be detected electrically. The appearance of a FRET signal in the donor channel parallel to the two electrical transitions clearly demonstrates the time correlation of both *structural* and *functional* transition. The reason for the missing optical counterpart to the first opening is most probably the limited observation region, leaving parts of the bilayer out of the window of observation.

SINGLE MOLECULE BINDING ASSAYS

In order to investigate receptor ligand binding on a single molecule level, we selected streptavidin as a test molecule. It is a bacterial protein that consists of four identical subunits, each binding one biotin with extremely high affinity (K_D=10fM [84]). Streptavidin was anchored to the lipid bilayer via biotinylated lipids at a low molar ratio [41]. Addition of a mixture of biotin and a long chain biotin-dye conjugate, biotin-PEG-TMR [85], resulted in statistical labeling of individual streptavidin molecules. The observed fluorescence signals of individual streptavidin molecules showed a much higher standard deviation compared to that of single dye molecules, a consequence of the statistical labeling pattern. Four equidistant peaks could be easily distinguished in the histogram, corresponding to N=1, 2, 3 or 4 bound biotin-dye molecules on a single streptavidin. The existence of signals at N>3 indicates dimerization of streptavidin molecules.

Still, the signal of two biotin-dye molecules bound to one streptavidin molecule is equivalent to the signal of two biotin-dye molecules bound to two distinct streptavidin molecules, which are accidentally located closer to each other than the diffraction limit. In order to rule out such accidental proximity as a cause for co-localization, we employed dual wavelength microscopy to improve the spatial resolution in such a binding assay [51]. A mixture of biotin-PEG-TMR and biotin-PEG-Cy5 was applied for streptavidin labeling. The low optical cross-talk allowed for selective excitation of only TMR (Cy5) upon illumination at 514nm (633nm). By toggling the excitation wavelength in a series of consecutive illuminations, images of TMR- and Cy5-labelled biotins could be obtained independently. From such images, the distance between two individual TMR and Cy5 labeled biotins was measured at a resolution of $\Delta d = \sqrt{2}\Delta r \approx 55nm$, clearly beyond the diffraction limit of light microscopy. In many cases, single TMR- and Cy5-labelled biotins were found to be closer than δd and thus have been ascribed to be bound to a single streptavidin molecule.

Fig. (3) shows an example for co-localization between fluorescence labeled biotin molecules on individual

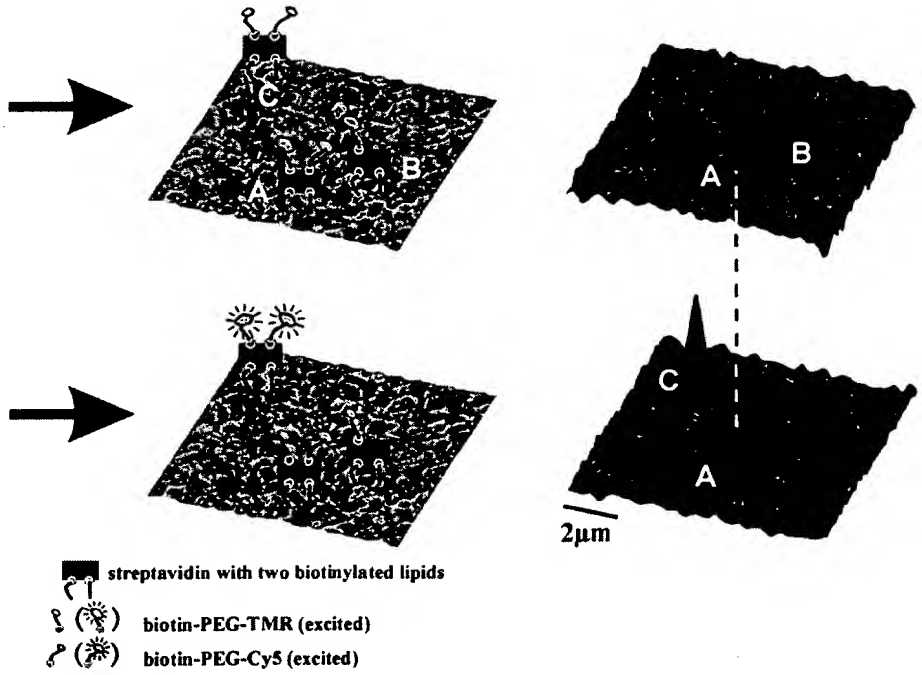

Fig. (3). Colocalization images of individual streptavidin molecules labeled with biotin-PEG-TMR and biotin-PEG-Cy5. Streptavidin was immobilized on a phospholipid bilayer using biotiniylated phospholipids. The same membrane area was illuminated consecutively for 35ms by 514nm (top) and 630nm light (bottom). On both images, two fluorescence peaks were observed, with one being colocalized within <30nm (A). This peak represents a single streptavidin molecule labled with one biotin-PEG-TMR and one biotin-PEG-Cy5 molecule. Additional information on the fluorescence signal allows to calculate the local stoichiometry on each streptavidin, as indicated on the left. Besides (A), the observed membrane area contains two additional streptavidin molecules labeled with biotins: One molecule (C) contains 2 biotin-PEG-Cy5, the second one only a single biotin-PEG-TMR (B) [51].

streptavidin molecules. Streptavidin was linked to a synthetic phospholipid bilayer via biotinylated lipid molecules (Schütz *et al.*, 1998). The two remaining binding pockets for biotin were labeled statistically with biotin-PEG-TMR and biotin-PEG-Cy5. Occasionally, two differently labeled biotin molecules were bound to a single streptavidin molecule. In these cases, we could determine the distance of the two biotin molecules with a precision down to ~40nm, limited only by the positional accuracy of the apparatus. This high positional accuracy enables the precise study of specific interactions between a ligand and its receptor in general, when the two molecules were labeled in a different color. Some fluorescence signals in Fig. (3), however, do not contain a counterpart in the second spectral channel. They are due to binding of only one biotin molecule, or of two biotins with the same color. By utilizing the fluorescence intensity as an information of the local stoichiometry, it was possible to distinguish between these cases and obtain the full characterization of the occupancy of all streptavidins observed (indicated on the left of Fig. (3)).

To extend the sensitive region for distance measurements into the nanometer range, the energy transfer from the donor molecule (TMR) to the acceptor (Cy5) has been studied. The strong distance dependency of FRET yielded detectable signals only in those cases, where donor and acceptor were located in close proximity, below the Förster distance of 7.6nm. This study gave definite proof for binding of single TMR- and Cy5-labelled biotins to the same streptavidin molecule.

A binding assay based on dual wavelength microscopy turned out to be an extremely sensitive method for the detection of specific binding events in a large background of unspecific adsorption. In a follow-up study, we could discriminate single oligonucleotide hybridization events out of a huge excess of unspecifically bound fluorescent oligonucleotides [86, 87]. Here, using a lipid bilayer as a matrix allowed for the full control over the surface density of biotinylated "capture" oligonucleotides, which have been anchored to the surface via TMR-labeled streptavidin and biotinylated lipids. Thus, the TMR-channel reported the position of capture DNA. The system has been incubated with Cy5-labelled oligonucleotides containing the complementary sequence. Hybridization events were easily detected by correlating the green and the red image. Statistical analysis showed the extremely high reliability in the detection of positive binding events [86].

The determination of pharmacologically relevant constants is crucial in order to understand the effects of compounds interacting with various membrane receptors. The natural system to measure such interactions, however, is the receptor within the plasma membrane of the living cell, and the externally applied ligand. We demonstrated that ultra-sensitive fluorescence microscopy can be used to determine ligand binding constants on a single cell level expressing as few as 100 receptor sites per cell [88]. The dissociation constant (K_D) and the off-rate (k_{off}) of $HgTX_1$-A19C-Cy5 [89] from its receptor, the $K_V1.3$ potassium channel, was determined on living Jurkat cells.

In principal, estimation of the average number of bound ligands at different concentrations of free ligand would allow the determination of the dissociation constant, K_D. However, variations in the expression level of $K_V1.3$ channels on different cells make this approach highly unreliable in experiments at low ligand concentration. To correct for this variation in channel densities, the fluorescence intensity F as a function of ligand concentration c was measured at a second ligand concentration, c_0, for each cell. The normalized value, $f = \frac{F(c)}{F(c_0)}$, is independent of the number of receptors per cell. Since the interaction between $HgTX_1$-A19C-Cy5 and $K_V1.3$ channels is of first order, this ratio is given by $f = 1 + \frac{K_D}{c_0} \Big/ 1 + \frac{K_D}{c}$. For high values of c, f approaches $1 + \frac{K_D}{c_0}$. Fig. (4) shows f as a function of the ligand concentration, with c_0 = 1nM. The data follow closely a hyperbolic function with K_D=280 ± 30 pM.

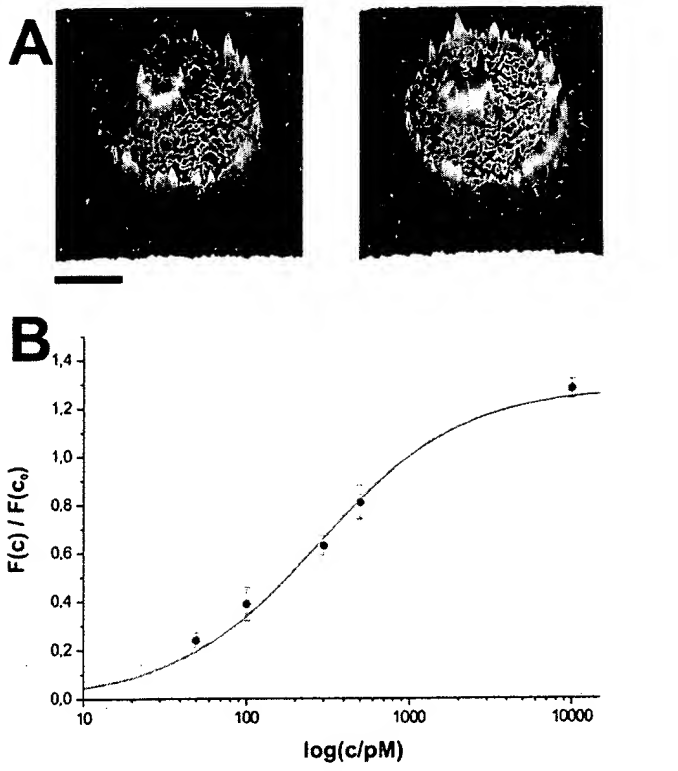

Fig. (4). A) Fluorescence image of a single Jurkat cell after specific labeling of the potassium channel $K_V1.3$ by $HgTX_1$-A19C-Cy5 at a concentration of c=300pM (left) and c_0=1nM (right). One can easily discriminate individual channel molecules distributed ununiformly over the plasma membrane. Upon increase in the ligand concentration, a concomitant rise in the number of fluorescently labeled channels can be observed (right image). The intracellular signal can be attributed to cellular autofluorescence. **B)** Fluorescence signal of labeled potassium channels as function of the $HgTX_1$-A19C-Cy5 concentration. Each data point represents the value normalized by the fluorescence signal obtained at c_0=1nM. The signals of 3 cells were used for averaging. Assuming a first order binding process, the dissociation constant was determined K_D= 280 ± 30pM. Bar 5μm. Reprinted by permission from Histochem. Cell Biol. [88], copyright 2002 by Springer-Verlag.

Single Molecule Reader for live cell imaging

The successful utilization of SDT for the study of model membranes yielded the promising perspective of a rather instantaneous application to living cells. However, the frequent occurrence of many species of endogenous fluorescent molecules inside cells made such an application difficult. Cellular autofluorescence has been characterized in terms of spectral properties [90], lifetime [91], and spatial distribution [92]. In the visible regime, flavins [90] and lipofuscin [93] are currently regarded as the major source of endogenous fluorescence. Flavins are mainly located in mitochondria, while lipofuscins predominantly reside in lysosomes. In fluorescence images, both organelles appear as diffraction-limited spots randomly distributed in the cytoplasm of the cell. The high variability of the fluorescence intensity of such spots, even within one cell, makes unambiguous distinction between fluorophores and autofluorescence a challenging task.

Our strategy for minimizing signal contributions due to autofluorescence was based on choosing long wavelengths for excitation. In the case of Human aorta smooth muscle (HASM) cells, no significant background has been observed at 633nm excitation [12]. As a continuation of our studies on artificial membranes, we introduced different types of fluorescence labeled lipids into the plasma membrane of those cells and recorded their mobility (Fig. (5)); the slightly decreased S/B reduced the positional accuracy to ~50nm. An interesting result was the qualitatively different behavior of the lipid probe when carrying different acyl chains. Using the fluorescent label Cy5, a lipid probe with mono-unsaturated acyl chains (1,2-dioleoyl-3-phosphoethanolamine-Cy5, DOPE-CY5) showed anomalous but unconfined diffusional motion, whereas a probe with fully saturated acyl chains (1,2-dimyristoyl-3-phosphoethanolamine, DMPE-Cy5) was found to be restricted to microdomains of ~700nm size, as determined by analysis of diffusion trajectories. These microdomains became directly visible at conditions of a few lipid probes per domain. In addition, the motion of the individual microdomains could be monitored by repeated imaging, partly as fluctuations around a central position, partly as unidirectional movement. This study made possible

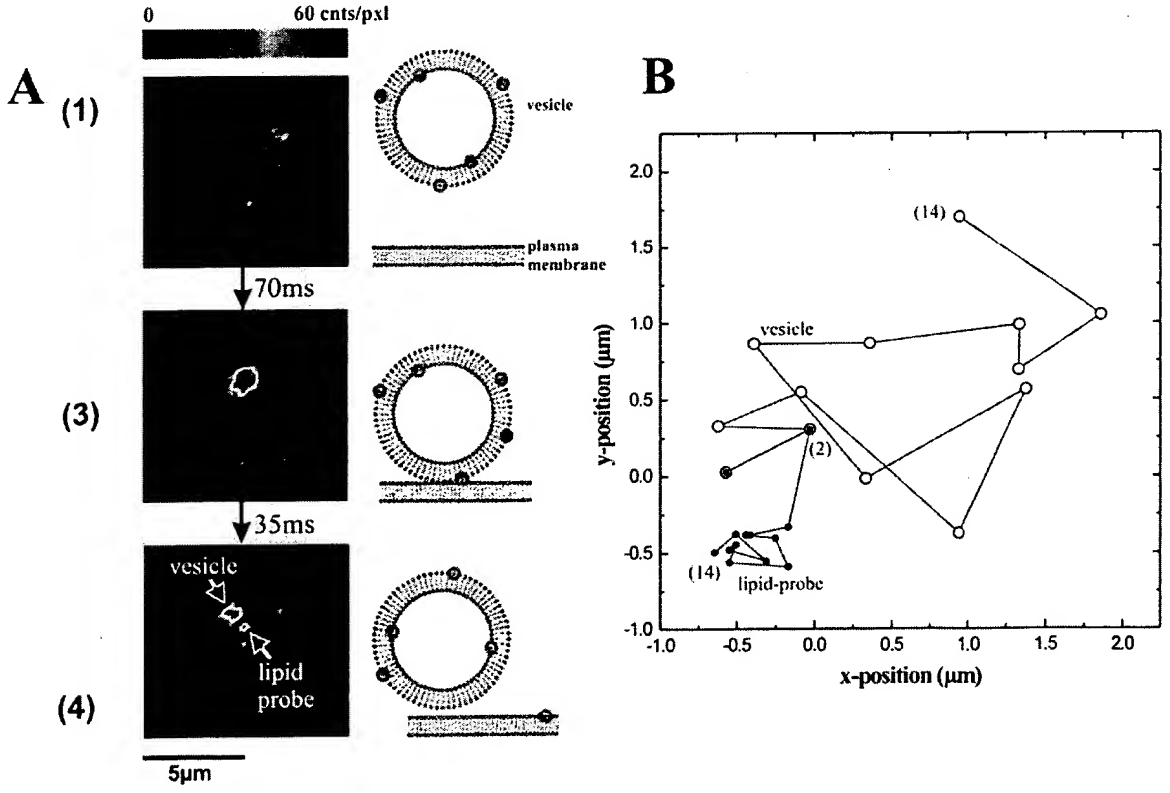

Fig. (5). A) Insertion of a single lipid probe molecule into the plasma membrane of a HASM cell. The fluorescence image shows an area of 10x10µm on the top surface of the cell. A very small number of vesicles containing DMPE-Cy5 as probe-lipid was applied. In the first image only a small fluorescence signal can be observed, corresponding to a vesicle entering the focal plane of the objective. After 70ms the vesicle, which can now be observed as a bright spot, has attached to the membrane. 35ms later a second, much smaller fluorescence signal appears, which represents the unitary intensity of a single DMPE-Cy5 molecule inserted into the plasma membrane. **B)** The trajectories of the lipid molecule (●) and the vesicle (○) have been reconstructed from a sequence of 14 consecutive images with a delay of 35ms. Before lipid insertion, positions (2) and (3), vesicle and lipid probe are still co-localized. After insertion, positions (4) to (14), the two trajectories reveal a much higher mobility of the vesicle compared to the lipid molecule. The images corresponding to positions (3) and (4) are shown in A. Reprinted by permission from EMBO J., [12], copyright 2000 by The European Molecular Biology Organization.

an *in vivo* characterization of lipid microdomains. Our results are not only in good agreement with corresponding biochemical data [94], they exceed biochemical studies by offering additional information on domain size and fluidity.

In the mean-time, several groups of scientists also succeeded in the successful application of single molecule microscopy to living cells [11, 95-100]. In most applications, autofluorescence turned out to be a severe limitation, especially in cases where the choice of the appropriate cell type is predetermined by the cell-biological problem. For such cases, we developed a method for the decomposition of optical signals originating from two spectrally distinct components: 1, a specific fluorophore, and 2, cellular autofluorescence [101]. Our method is based on the more general algorithm of singular value decomposition [102]. Two distinct spectral channels are recorded in parallel: a "green" channel, containing signals from both the introduced fluorophore and autofluorescence, and a "red" channel, with only autofluorescence contributions. Even at signal levels typical for single molecule microscopy, clear discrimination was feasible.

OUTLOOK

The increased information content of single molecule measurements compared to experiments on ensembles of molecules allows to design novel types of assays. Additional screening parameters come into reach, like receptor occupancies, colocalization of different ligands on one receptor, or even details like receptor-ligand-orientations. The full impact of this new information for drug-screening – but also medical diagnostics – has yet to be proven. Single molecule screening techniques have shown their feasibility for routine measurements in a scientific environment; for their general application, however, easy-to-use systems still have to be developed. In combination with novel software algorithms, ultra-sensitive imaging techniques are foreseen to become standard equipment for laboratories performing biological diagnostics.

ACKNOWLEDGEMENTS

This work was funded by the Austrian Federal Ministry of Education, Science and Culture, by the State of Upper Austria, and by the Austrian Research Funds.

REFERENCES

[1] Schweitzer, B.; Roberts, S.; Grimwade, B.; Shao, W.; Wang, M.; Fu, Q.; Shu, Q.; Laroche, I.; Zhou, Z.; Tchernev, V. T.; Christiansen, J.; Velleca, M.; Kingsmore, S. F. *Nat. Biotechnol.*, **2002**, *20*, 359-65.

[2] Zhang, Z.; Krylov, S.; Arriaga, E. A.; Polakowski, R.; Dovichi, N. *J. Anal. Chem.*, **2000**, *72*, 318-22.

[3] Pawlak, M.; Schick, E.; Bopp, M. A.; Schneider, M. J.; Oroszlan, P.; Ehrat, M. *Proteomics*, **2002**, *2*, 383-393.

[4] Weiss, S. *Science*, **1999**, *283*, 1676-83.

[5] Moerner, W. E.; Orrit, M. *Science*, **1999**, *283*, 1670-6.

[6] Moerner, W. E.; Kador, L. *Physical Review Letters*, **1989**, *62*, 2535-2538.

[7] Shera, E. B.; Seitzinger, N. K.; Davis, L. M.; Keller, R. A.; Soper, S. A. *Chemical Physics Letters*, **1990**, *174*, 553-557.

[8] Sase, I.; Miyata, H.; Corrie, J. E.; Craik, J. S.; Kinosita, K. Jr. *Biophys. J.*, **1995**, *69*, 323-8.

[9] Funatsu, T.; Harada, Y.; Tokunaga, M.; Saito, K.; Yanagida, T. *Nature*, **1995**, *374*, 555-9.

[10] Schmidt, T.; Schutz, G. J.; Baumgartner, W.; Gruber, H. J.; Schindler, H. *Proc. Natl. Acad. Sci. USA*, **1996**, *93*, 2926-9.

[11] Sako, Y.; Minoghchi, S.; Yanagida, T. *Nat. Cell Biol.*, **2000**, *2*, 168-72.

[12] Schutz, G. J.; Kada, G.; Pastushenko, V. P.; Schindler, H. *EMBO J.*, **2000**, *19*, 892-901.

[13] Schutz, G. J.; Pastushenko, V. P.; Gruber, H. J.; Knaus, H.-G.; Pragl, B.; Schindler, H. *Single Mol.*, **2000**, *1*, 25-31.

[14] Nie, S.; Chiu, D. T.; Zare, R. N. *Science*, **1994**, *266*, 1018-21.

[15] Bismuto, E.; Gratton, E.; Lamb, D. C. *Biophys. J.*, **2001**, *81*, 3510-21.

[16] Wennmalm, S.; Edman, L.; Rigler, R. *Proc. Natl. Acad. Sci. USA*, **1997**, *94*, 10641-6.

[17] Eggeling, C.; Berger, S.; Brand, L.; Fries, J. R.; Schaffer, J.; Volkmer, A.; Seidel, C. A. *J. Biotechnol.*, **2001**, *86*, 163-80.

[18] Haupts, U.; Maiti, S.; Schwille, P.; Webb, W. W. *Proc. Natl. Acad. Sci. USA*, **1998**, *95*, 13573-8.

[19] Korlach, J.; Schwille, P.; Webb, W. W.; Feigenson, G. W. *Proc. Natl. Acad. Sci. USA*, **1999**, *96*, 8461-6.

[20] Krichevski, O.; Bonnet, G. *Reports on Progress in Physics*, **2002**, *65*, 251-297.

[21] Auer, M. *Drug Discov. Today*, **2001**, *6*, 935-936.

[22] Van Orden, A.; Keller, R. A.; Ambrose, W. P. *Anal. Chem.*, **2000**, *72*, 37-41.

[23] Minsky, M. *Scaninng*, **1988**, *10*, 128-138.

[24] Pawley, J. B. *Handbook of Biological Confocal Microscopy*, New York: Plenum **1995**.

[25] Xu, X. H.; Yeung, E. S. *Science*, **1997**, *275*, 1106-9.

[26] Dickson, R. M.; Cubitt, A. B.; Tsien, R. Y.; Moerner, W. E. *Nature*, **1997**, *388*, 355-8.

[27] Dickson, R. M.; Norris, D. J.; Tzeng, Y. L.; Moerner, W. E. *Science*, **1996**, *274*, 966-9.

[28] Schmidt, T.; Schutz, G. J.; Baumgartner, W.; Gruber, H. J.; Schindler, H. *J. Phys. Chem.*, **1995**, *99*, 17662-17668.

[29] Hecht, E. *Optics*, Addison-Wesley: Reading **1987**.

[30] Cheezum, M. K.; Walker, W. F.; Guilford, W. H. *Biophys. J.*, **2001**, *81*, 2378-88.

[31] Bobroff, N. *Rev. Sci. Instrum.*, **1986**, *57*, 1152-1157.

[32] Thompson, R. E.; Larson, D. R.; Webb, W. W. *Biophys. J.*, **2002**, *82*, 2775-83.

[33] Schutz, G. J.; Schindler, H.; Schmidt, T. *Biophys. J.*, **1997**, *73*, 1073-80.

[34] Yildiz, A.; Forkey, J. N.; McKinney, S. A.; Ha, T.; Goldman, Y. E.; Selvin, P. R. *Science*, **2003**, *300*, 2061-5.

[35] Chandrasekar, S. *Rev. Mod. Phys.*, **1943**, *15*, 1-89.

[36] Hellen, E. H., Axelrod, D. *Review of Scientific Instruments*, **1990**, *61*, 3722.

[37] Knemeyer, J. P.; Herten, D. P.; Sauer, M. *Anal. Chem.*, **2003**, *75*, 2147-53.

[38] Filippova, E. M.; Monteleone, D. C.; Trunk, J. G.; Sutherland, B. M.; Quake, S. R.; Sutherland, J. C. *Biophys. J.*, **2003**, *84*, 1281-90.

[39] Goodwin, P. M.; Johnson, M. E.; Martin, J. C.; Ambrose, W. P.; Marrone, B. L.; Jett, J. H.; Keller, R. A. *Nucleic Acids Res.*, **1993**, *21*, 803-6.

[40] Gross, D.; Webb, W. W. *Biophys. J.*, **1986**, *49*, 901-11.

[41] Schmidt, T.; Schutz, G. J.; Gruber, H. J.; Schindler, H. *Anal. Chem.*, **1996**, *68*, 4397-4401.

[42] Ha, T.; Enderle, T.; Ogletree, D. F.; Chemla, D. S.; Selvin, P. R.; Weiss, S. *Proc. Natl. Acad. Sci. USA*, **1996**, *93*, 6264-8.

[43] Ha, T.; Enderle, T.; Chemla, D. S.; Weiss, S. *IEEE J. Sel. Top. Q.E.*, **1996**, *2*, 1-14.

[44] Förster, T. *Ann. Physik*, **1948**, *6*, 55-75.

[45] Kenworthy, A. K.; Edidin, M. *J. Cell Biol.*, **1998**, *142*, 69-84.

[46] Taylor, D. L.; Wang, Y.-L. *Fluorescence microscopy of living cells in culture Part B*, San Diego Academic Press **1989**.

[47] Mahajan, N. P.; Linder, K.; Berry, G.; Gordon, G. W.; Heim, R.; Herman, B. *Nat. Biotechnol.*, **1998**, *16*, 547-52.

[48] Ha, T. *Methods*, **2001**, *25*, 78-86.

[49] Deniz, A. A.; Dahan, M.; Grunwell, J. R.; Ha, T.; Faulhaber, A. E.; Chemla, D. S.; Weiss, S.; Schultz, P. G. *Proc. Natl. Acad. Sci. USA*, **1999**, *96*, 3670-5.

[50] Ha, T.; Ting, A. Y.; Liang, J.; Caldwell, W. B.; Deniz, A. A.; Chemla, D. S.; Schultz, P. G.; Weiss, S. *Proc. Natl. Acad. Sci. USA*, **1999**, *96*, 893-8.

[51] Schutz, G. J.; Trabesinger, W.; Schmidt, T. *Biophys. J.*, **1998**, *74*, 2223-6.

[52] Enderle, T.; Ha, T.; Chemla, D. S.; Weiss, S. *Ultramicroscopy*, **1998**, *71*, 303-9.
[53] Cognet, L.; Harms, G. S.; Blab, G. A.; Lommerse, P. H.; Schmidt, T. *Appl. Phys. Lett.*, **2000**, *77*, 1-3.
[54] Saito, K.; Tokunaga, M.; Iwane, A. H.; Yanagida, T. *J. Microsc.*, **1997**, *188*, 255-63.
[55] Ha, T.; Enderle, T.; Chemla, S.; Selvin, R.; Weiss, S. *Physical Review Letters*, **1996**, *77*, 3979-3982.
[56] Güttler, F.; Sepiol, J.; Plakhotnik, T.; Mitterdorfer, A.; Renn, A.; Wild, U. P. *J. Luminescence*, **1993**, *56*, 29-38.
[57] Ruiter, A. G. T.; Verman, J. A.; Garcia-Parajo, M. F.; van Hulst, N. F. *J. Phys. Chem.*, **1997**, *101*, 7318-7323.
[58] Schutz, G. J.; Schindler, H.; Schmidt, T. *Opt. Lett.*, **1997**, *22*, 651-653.
[59] Sase, I.; Miyata, H.; Ishiwata, S.; Kinosita, K., Jr. *Proc. Natl. Acad. Sci. USA*, **1997**, *94*, 5646-50.
[60] Warshaw, D. M.; Hayes, E.; Gaffney, D.; Lauzon, A. M.; Wu, J.; Kennedy, G.; Trybus, K.; Lowey, S.; Berger, C. *Proc. Natl. Acad. Sci. USA*, **1998**, *95*, 8034-9.
[61] Harms, G. S.; Sonnleitner, M.; Schutz, G. J.; Gruber, H. J.; Schmidt, T. *Biophys. J.*, **1999**, *77*, 2864-70.
[62] Ha, T.; Glass, J.; Enderle, T.; Chemla, D. S.; Weiss, S. *Phys. Rev. Lett.*, **1998**, *80*, 2093-2096.
[63] Veerman, J. A.; Garcia-Parajo, M. F.; Kuipers, L.; van Hulst, N. F. *J. Microsc.*, **1999**, *194 (Pt 2-3)*, 477-82.
[64] Betzig, E.; Chichester, R. J. *Science*, **1993**, *262*, 1422-1425.
[65] Sick, B.; Hecht, B.; Novotny, L. *Phys. Rev. Lett.*, **2000**, *85*, 4482-5.
[66] Singer, S. J.; Nicolson, G. L. *Science*, **1972**, *175*, 720-31.
[67] Selig, J. In *Physical properties of model membranes and biological membranes*, R. Balian, ed.; North Holland, **1981**, pp. 16-78.
[68] Qian, H.; Sheetz, M. P.; Elson, E. L. *Biophys. J.*, **1991**, *60*, 910-21.
[69] Saxton, M. J. *Biophys. J.*, **1993**, *64*, 1766-80.
[70] Saxton, M. J. *Biophys. J.*, **1995**, *69*, 389-98.
[71] Sheets, E. D.; Lee, G. M.; Simson, R.; Jacobson, K. *Biochemistry*, **1997**, *36*, 12449-58.
[72] Huang, Z.; Pearce, K. H.; Thompson, N. L. *Biochim. Biophys. Acta*, **1992**, *1112*, 259-65.
[73] Tamm, L. K. *Biochemistry*, **1988**, *27*, 1450-7.
[74] Sonnleitner, A.; Schutz, G. J.; Schmidt, T. *Biophys. J.*, **1999**, *77*, 2638-42.
[75] Timbs, M. M.; Thompson, N. L. *Biophys. J.*, **1990**, *58*, 413-28.
[76] Timbs, M. M.; Thompson, N. L. *Biopolymers*, **1993**, *33*, 45-57.
[77] Bernsdorff, C.; Wolf, A.; Winter, R.; Gratton, E. *Biophys. J.*, **1997**, *72*, 1264-77.
[78] Hille, B. *Ionic Channels of excitable membranes*, Sinauer Ass.: Sunderland **1984**.
[79] Poste, G.; Nicolson, G. L. eds. *Membrane Reconstitution*, North-Holland Publishing Company: Amsterdam\ **1982**.
[80] Cha, A.; Snyder, G. E.; Selvin, P. R.; Bezanilla, F. *Nature*, **1999**, *402*, 809-13.
[81] Glauner, K. S.; Mannuzzu, L. M.; Gandhi, C. S.; Isacoff, E. Y. *Nature*, **1999**, *402*, 813-7.
[82] Borisenko, V.; Lougheed, T.; Hesse, J.; Fureder-Kitzmuller, E.; Fertig, N.; Behrends, J. C.; Woolley, G. A.; Schutz, G. J. *Biophys. J.*, **2003**, *84*, 612-22.
[83] Woolley, G. A.; Wallace, B. A. *J. Membr. Biol.*, **1992**, *129*, 109-36.
[84] Wilcheck, M.; Bayer, E. A. eds. *Avidin-biotin technology*, Academic Press: San Diego\ **1990**.
[85] Haselgrubler, T.; Amerstorfer, A.; Schindler, H.; Gruber, H. J. *Bioconjug. Chem.*, **1995**, *6*, 242-8.
[86] Trabesinger, W.; Hecht, B.; Wild, U. P.; Schutz, G. J.; Schindler, H.; Schmidt, T. *Anal. Chem.*, **2001**, *73*, 1100-5.
[87] Trabesinger, W.; Schutz, G. J.; Gruber, H. J.; Schindler, H.; Schmidt, T. *Anal. Chem.*, **1999**, *71*, 279-83.
[88] Freudenthaler, G.; Axmann, M.; Schindler, H.; Pragl, B.; Knaus, H. G.; Schutz, G. J. *Histochem. Cell Biol.*, **2002**, *117*, 197-202.
[89] Koschak, A.; Bugianesi, R. M.; Mitterdorfer, J.; Kaczorowski, G. J.; Garcia, M. L.; Knaus, H.-G. *J. Biol. Chem.*, **1998**, *273*, 2639-2644.
[90] Benson, R. C.; Meyer, R. A.; Zaruba, M. E.; McKhann, G. M. *J. Histochem. Cytochem.*, **1979**, *27*, 44-48.
[91] Konig, K.; So, P. T.; Mantulin, W. W.; Tromberg, B. J.; Gratton, E. *J. Microsc.*, **1996**, *183*, 197-204.
[92] Andersson, H.; Baechi, T.; Hoechl, M.; Richter, C. *J. Microsc.*, **1998**, *191*, 1-7.
[93] Schnell, S. A.; Staines, W. A.; Wessendorf, M. W. *J. Histochem. Cytochem.*, **1999**, *47*, 719-30.
[94] Schroeder, R.; London, E.; Brown, D. *Proc. Natl. Acad. Sci. USA*, **1994**, *91*, 12130-4.
[95] Kues, T.; Dickmanns, A.; Luhrmann, R.; Peters, R.; Kubitscheck, U. *Proc. Natl. Acad. Sci. USA*, **2001**, *98*, 12021-6.
[96] Ueda, M.; Sako, Y.; Tanaka, T.; Devreotes, P.; Yanagida, T. *Science*, **2001**, *294*, 864-7.
[97] Seisenberger, G.; Ried, M. U.; Endress, T.; Buning, H.; Hallek, M.; Brauchle, C. *Science*, **2001**, *294*, 1929-32.
[98] Kues, T.; Peters, R.; Kubitscheck, U. *Biophys. J.*, **2001**, *80*, 2954-67.
[99] Iino, R.; Koyama, I.; Kusumi, A. *Biophys. J.*, **2001**, *80*, 2667-77.
[100] Harms, G. S.; Cognet, L.; Lommerse, P. H.; Blab, G. A.; Kahr, H.; Gamsjager, R.; Spaink, H. P.; Soldatov, N. M.; Romanin, C.; Schmidt, T. *Biophys. J.*, **2001**, *81*, 2639-46.
[101] Moertelmaier, M. A.; Kögler, E. J.; Hesse, J.; Sonnleitner, M.; Huber, L. A.; Schütz, G. J. *Single Mol.*, **2002**, *3*, 225-231.
[102] Frederix, P. L. T. M.; Asselbergs, M. A. H.; van Sark, W. G. J. H. M.; van den Heuvel, D. J.; Hamelink, W.; de Beer, E. L.; Gerritsen, H. C. *Appl. Spectr.*, **2001**, *55*, 1005-1012.

APPENDIX C

"Single-Molecule Reader for Proteomics and Genomics" by Hesse, *et al.*, J. Chromatography B 782 (2002):127-135

ELSEVIER

Journal of Chromatography B, 782 (2002) 127–135

JOURNAL OF CHROMATOGRAPHY B

www.elsevier.com/locate/chromb

Review

Single-molecule reader for proteomics and genomics

Jan Hesse[a], Christian Wechselberger[b], Max Sonnleitner[b], Hansgeorg Schindler[a], Gerhard J. Schütz[a,*]

[a]*Biophysics Institute, Johannes-Kepler-University Linz, Altenbergerstrasse 69, A-4040 Linz, Austria*
[b]*Center for Biomedical Nanotechnology, Upper Austrian Research GmbH, Scharitzerstrasse 6-8, A-4020 Linz, Austria*

Abstract

Recent developments in ultrasensitive fluorescence microscopy enabled the detection and detailed characterization of individual biomolecules in their native environment. New types of information can be obtained from studying individual molecules, which is not accessible from ensemble measurements. Moreover, this methodological advance matches the need of bioscience to downscale the sample amount required for screening devices. It is envisioned that concentrations as low as ~1000 molecules contained in a sample of 1 nl can be detected in a chip-based assay. In this review, we overview state-of-the-art single molecule microscopy with respect to its applicability to ultrasensitive screening. Quantitative estimations will be given, based on a novel apparatus designed for large area screening at single molecule sensitivity.

Keywords: Reviews; Proteomics; Genomics; Single-molecule reader

Contents

1. Introduction

Insights into biological properties of cells are commonly gained through the determination of RNA and protein expression profiles. Phenotypic aberrations have been shown to be directly linked to the expression of specific genes or proteins [1]. These correlations represent the basis for current assays in bioscience and medical diagnostics. Unambiguous identification of aberrant phenotypes, still, remains a

*Corresponding author. Tel.: +43-732-2468-9265; fax: +43-732-2468-9280.
E-mail address: gerhard.schuetz@jku.at (G.J. Schütz).

1570-0232/02/$ – see front matter
PII: S1570-0232(02)00552-4

difficult task. Large amounts of sample material are required in order to yield detectable signals. This requirement is not limiting for the study of model systems, which use cell culture systems. In contrast, only minute amounts of tissue or body fluids are available for routine sample screening in medical diagnostics. For nucleic acid detection, the problem of limited sample size can be bypassed using PCR-based amplification. Such methods, however, often lead to complications due to cross-contamination of sample material, and distorted statistical outputs. On the contrary, for the analysis of proteins only indirect amplification methods exist [2].

From this line of argumentation, an ultra-sensitive detection device is mandatory for any future genomics and proteomics platform. Steps towards this direction have been taken using gel electrophoresis [3], which allowed to quantify protein expression on single cells. In a different approach, highly sensitive protein-chip read-out has been accomplished using excitation via a planar wave-guide [4]. Recent advances in fluorescence detection techniques extended the range of sensitivity down to the level of single dye molecules. Using such devices, reliable quantification of the number of analytes immobilized on a chip surface is possible at a high dynamic range, from ~10^6 molecules down to 1 molecule per 100 μm^2. In order to make such detection devices applicable for diagnostic purposes, high throughput capability has to be ensured. Scanning speeds up to 1 cm^2 within ~15 min are feasible with current detectors. In this review, we summarize recent developments in ultra-sensitive high-throughput fluorescence detection in view of its applicability to current demands in genomics and proteomics.

2. Methods for the detection of single molecules

Pioneering work for the detection and characterization of single fluorescent molecules was performed in the early 1990s by several groups, which studied the spectroscopic behavior of single chromophores embedded in condensed matter at low temperature [5,6]. These studies pushed the limits of sensitivity, however, the systems investigated were far from being biologically relevant. Milestones on the way to applicability in bioscience were reached during the last decade, including single molecule detection at room temperature [7], in buffer [8–10], and in living cells [11–13].

Currently, two strategies are followed for establishing high-throughput screening devices at single molecule sensitivity: firstly, fluorescent molecules in solution are detected by a stationary excitation and detection system. Most prominently, confocal devices have been applied to restrict the detection volume down to a few femtoliters [14]. Using avalanche photodiodes as detectors allows to study the fluorescence intensity, fluorophore transition rates and spatial mobility. Combination of multiple detectors gains additional information about spectral properties. Such devices have been extensively used to study binding kinetics [15], conformational fluctuations [16], spectroscopic transitions [17,18] and molecular mobilities [19] using fluorescence correlation spectroscopy (FCS, for a review see Ref. [20]). This information can be assessed within a few seconds, rendering FCS a promising tool for miniaturized high-throughput screening [21]. Fluorescent molecules in solution have been directly imaged on a camera, as they were passing through the defocused excitation beam. The largely increased observation area, compared to a point detector as used for FCS, highly increases detection speed, which has been utilized for DNA fragment sizing [22]. Constant flow of the solution and hydrodynamic focusing ensure that most molecules will pass the detection volume, making this method applicable for detection of trace amounts of molecules.

Secondly, surface-immobilized molecules can be detected using screening stages. For this purpose, distinct areas of a glass surface are functionalized with capture agents, e.g. antibodies, specific ligands, or cDNA. This procedure allows for parallel investigation of a large number of different fluorescence labeled target molecules on one chip. The basis for ultra-sensitive chip read-out are techniques for detecting single molecules on surfaces. In initial studies, confocal microscopy was used to efficiently discriminate single molecule signals from background. The method is based on scanning a diffraction limited laser focus over the sample; the fluorescence emitted from the sample is imaged via a

pinhole onto a point detector [23,24]. Using Avalanche Photodiodes (APD) as detectors allows to obtain additional information about the excited state lifetime. Combination of several APDs placed after a stack of dichroic and polarization beam splitters was used to maximize the information content acquired from a single molecule [17]. However, due to the serial data acquisition the inspection of large sample areas remains a time-consuming task. The time T required for recording an area A at a resolution δ and an illumination time t_{ill} can be calculated according to $T = A/\delta^2\, t_{ill}$. For $\delta = 320$ nm and $t_{ill} = 10$ ms, the time for recording an area $A = 1$ cm^2 in a confocal set-up is equal to 9.9×10^6 s (corresponding to 3.8 months).

In a different approach, several groups utilized intensified or back-illuminated CCD-cameras for imaging single molecules on surfaces [8–10,25–27]. Large sample areas are illuminated with a defocused laser spot and directly imaged. This simultaneous observation was the methodological prerequisite for tracking individual molecules moving in planar systems. In screening assays, parallel observation of many pixels dramatically reduces the recording time T, compared to confocal methods. T can be estimated using the formula $T = A/\delta^2 N \cdot [t_{ill} + Nt_{read\text{-}out} + Lt_{line\text{-}shift} + t_{positioning}]$, with N the overall number of pixels on the camera chip. The sum represents contributions of the illumination time (t_{ill}), the time to digitize each pixel ($t_{read\text{-}out}$), the time to shift one line into the read-out register ($t_{line\text{-}shift}$) and additional terms accounting for positioning the stage, subsumed in $t_{positioning}$; L gives the total number of lines on the chip.

The principal advantage of using pixel arrays as detectors is parallel signal acquisition. Still, the pixel array covers only a small part of the sample area A to be imaged, making additional scanning of the sample inevitable. A proper way for reducing overhead times due to stage positioning and signal integration is the implementation of synchronized continuous stage-shift and camera read-out (H. Schindler, international patent PCT/AT9900257). It is based on the so-called time-delayed-integration (TDI) mode, and allows to decrease the recording time to $T = A/\delta^2 N \cdot [Nt_{read\text{-}out} + Lt_{line\text{-}shift}] \approx 1000$ s, corresponding to 16.7 min (assuming a commercial available NTE/CCD 1340×100, Roper Scientific, with $t_{read\text{-}out} = 1$ μs and $t_{line\text{-}shift} = 12$ μs). In the direction of scanning, the intensity profile of the excitation beam needs not to be constant. In practice, it is convenient to use a Gaussian profile with a width of $\omega \approx L\delta/2$. This ensures maximum excitation of dye molecules within the region of observation, and at the same time minimum photobleaching of dyes in regions still to be scanned. In TDI mode, the illumination time is not well-defined. Basically, it is given by the time required to move each molecule through the excitation beam. In order to allow comparison between TDI mode and conventional imaging, we define here an effective illumination time for TDI mode, $\hat{t}_{ill}$: given an image recorded in TDI mode, $\hat{t}_{ill}$ represents the illumination time in conventional imaging for recording an image of the same quality. Or, in mathematical terms: if $n_h = I_{max} t_{ill}$ represents the number of excitation cycles in a homogenous excitation beam profile of intensity I_{max}, and $n_i = \int I(x)\, dt$ the number of excitation cycles in TDI mode, the effective illumination time is given by the time for which n_h equals n_i, i.e. $n_h(\hat{t}_{ill}) = n_i$. Assuming a Gaussian beam profile with $I(x) = I_{max} \exp\left[-x^2/\omega^2\right]$, the effective illumination time is given by $\hat{t}_{ill} = I_{max}/\int I(x)/v\ dx = \sqrt{\pi}\omega/v = \sqrt{\pi}\omega/\delta L \cdot [Nt_{read\text{-}out} + Lt_{line\text{-}shift}]$. For the NTE/CCD 1340×100, $\hat{t}_{ill}$ equals 60 ms.

If the fluorescence intensity, F, would scale linearly with illumination intensity, I, i.e. $F \propto It_{ill}$, confocal scanning microscopy could be performed at the same speed as camera-based systems. In this linear regime, focusing of the laser spot by a factor N yields an increased excitation intensity NI, which allows to reduce t_{ill} by a factor N for constant fluorescence emission. However, for high speed single molecule detection it is favorable to operate at illumination intensities close to the saturation intensity of the fluorophore I_S, i.e. $F \propto (1 + I_S/I)^{-1} t_{ill}$ [28]. In this case, increase of the intensity has minor effects on F, therefore the illumination time may not be reduced in order to ensure constant signal. Evidently, non-linear effects make camera-based detection systems preferential for ultra-sensitive high-throughput screening. It is interesting to note, that for conventional dyes used in ultra-sensitive spectroscopy, the time required to photobleach the fluorophore at illumination intensities close to I_S is shorter than $\hat{t}_{ill}$ [29]. Therefore, all photons emitted from a molecule until

photobleaching contribute to the signal, yielding maximum signal levels.

The image of a single dye molecule is represented by a diffraction limited spot on the camera. Automatic fitting algorithms have been developed which allow to determine the position of individual molecules to an accuracy of ~50 nm. For unambiguous single molecule probing, the concentration has to be much less than $1/\delta^2$ to ensure that the signals of two molecules do not overlap. Assuming equal distribution of molecules on a surface, the probability that the distance to the nearest neighbor is larger than the size of the diffraction limited spot of $r = 500$ nm is given by $F_{nn}(r) = \exp(-r^2 \pi n)$ [30], with n the concentration of dye molecules. For a certainty $F > 95\%$, n has to be less than 1 molecule/15 μm^2.

In order to achieve single molecule sensitivity, the transmission efficiencies of all optical elements in the detection path have to be maximized. In general, the overall detection efficiency, η, can be separated into three factors: the efficiency of the microscope objective, η_O, of optical filters, η_F, and of the detector, η_D. Typical values are: $\eta_O \sim 30\%$ for an oil immersion objective with NA = 1.4, $\eta_F \sim 50\%$, $\eta_D \sim 80\%$, yielding $\eta \sim 12\%$. Obviously, the limiting factor is the objective, which collects only a minor fraction of all emitted photons due to the limited collection angle set by the numerical aperture. At optimized settings, such systems allow to obtain images of single dye molecules in synthetic environments at a high signal to background ratio of ~50. Besides high detection efficiencies, this is mainly related to the low noise characteristics of cooled CCD cameras.

Fig. 1 shows a schematic view of the apparatus developed in our lab, here termed "Nanoreader": laser light is coupled into an epi-fluorescence microscope, and the emitted light is detected after appropriate filtering on the pixel array of a CCD camera. The excitation beam is defocused to match the region of observation defined by the size of the CCD-array and the chosen magnification of the objective. A homogenous beam profile perpendicular to the scanning direction is achieved using an aspherical lens as beam shaper. For optimum resolution, the step-size of the high precision scanning stage has to fit the pixel size in the image plane, δ. In addition, an

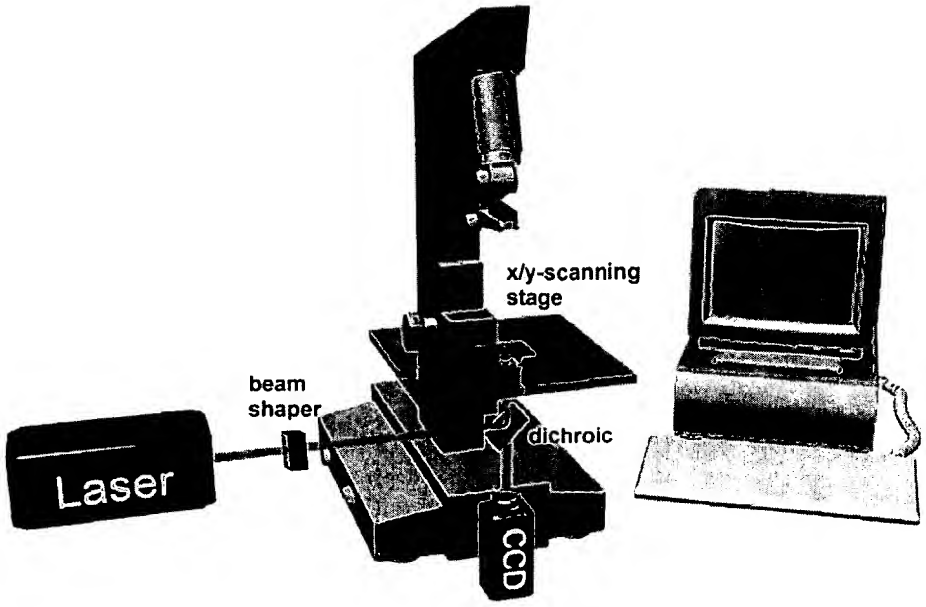

Fig. 1. Scheme showing the general set-up of the "Nanoreader". The laser beam is shaped with aspherical lenses to the desired line-profile, and projected onto the sample. Fluorescence emission is collected through a high NA objective and, after appropriate filtering, imaged onto a back-illuminated high QE CCD camera. For TDI mode, a high precision scanning stage is synchronized with the read-out of the camera.

autofocus system was introduced to correct for thickness-variations or tilts of the supporting chip-surface. It is based on rapidly refocusing the microscope objective during the scan process. Distance changes of the glass surface from the objective are measured using a second laser at a different wavelength focused onto the chip surface. Angular changes of the back-reflected beam are detected on a two-segment photodiode and corrected by shifting the objective [31].

Lipid bilayers represent a highly defined model system for single molecule microscopy [32]. They allow to precisely adjust the surface density down to very low concentrations of about one fluorescent molecule per 100 μm^2. Fig. 2 shows a supported lipid bilayer made of dipalmitoylphosphocholine (DPPC), containing a molar ratio of $\sim 10^{-8}$ of the fluorescent analog dipalmitoylphosphoethanolamine-(DPPE-) Cy5. An area of 200×600 μm was recorded in one scan using TDI-mode (A). The main part of the scan area is covered by the bilayer. There, individual DPPE-Cy5 molecules can easily be discriminated as sharp peaks with a signal-to-noise ratio of ~50 in the zoom-in (B). A few aggregates, however, can be observed as signals of much higher brightness in (A).

The scanning process introduces minor distortions broadening the peaks in the scanning direction by ~200 nm (C). Two major contributions for peak broadening have to be considered. Firstly, the scanning stage moves continuously, while lines are shifted stepwise on the CCD chip, which introduces blur of up to 1 pixel in the scanning direction. Secondly, non-perfect mechanics and optics might account for slight dephasing of the scanning stage and the CCD-camera. This effect can be minimized

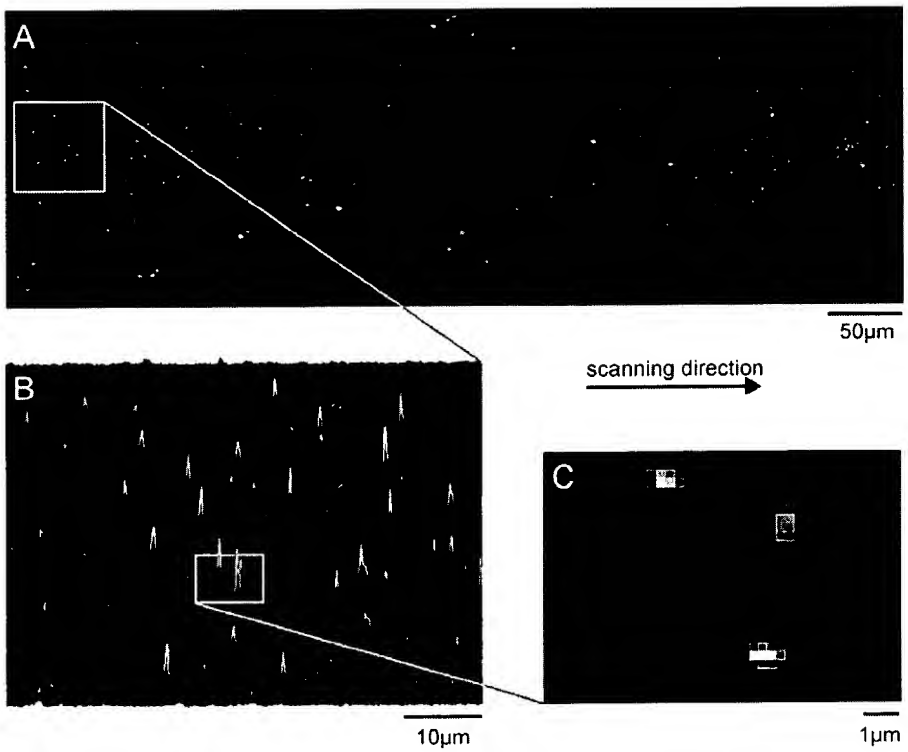

Fig. 2. A 200×600 μm scan (A) of single Cy5-labeled lipid molecules (DPPE-Cy5) embedded in a supported lipid membrane of DPPC, obtained with the "Nanoreader". The molar ratio of $\sim 10^{-8}$ allows to easily discriminate individual molecules as diffraction limited peaks at a signal to background ratio of ~50, as apparent from the 60×60 μm detail shown in (B). Due to the scanning process, the peak shape is slightly broadened in the scanning direction by ~200 nm (C; see text for details).

by adjusting the magnification of the optical system to fit the demands set by the scanning stage.

3. Information contained in single molecule images

The fluorescence image of a dye molecule contains two parameters accessible by a camera as a detector: firstly, the *position* of the molecule, which is given by the center of its signal. This can be determined to an accuracy much below the wavelength of light; ~40 nm can be achieved routinely for positioning single biomolecules at room temperature using wide field microscopy [33]. Secondly, its *fluorescence intensity*, which can be quantified by the number of photons detected from the molecule during the illumination time. This number can be taken as a characteristic property of the dye molecule under constant environmental conditions. A third parameter, the *fluorescence lifetime*, is up to now only measurable using point detectors; for a critical discussion of the implications of lifetime analysis for single molecule studies we refer to Refs. [6,17]. In the following, several aspects of single molecule studies based on these observables will be highlighted.

3.1. Local stoichiometry

In general, a single dye molecule emits a well-defined number of photons during a given illumination time, which can be taken as a characteristic parameter of the molecule. The fluorescence signal obtained from a single molecular structure can thus be used as a measure for the number of bound fluorophores. This principle has been employed in rather different fields like rapid sizing of fluorescently stained DNA-fragments [34], as well as molecular counting of low-density lipoprotein particles on cell surfaces [35]. The critical point in all methodologies utilizing fluorescence intensity for sizing is the reliability of assignment. Using randomly labeled particles, the accuracy of discrimination between n and $n+1$ associated particles scales with $N^{0.5}$, with N representing the mean number of fluorophores per particle. Therefore, high discrimination accuracy requires heavily labeled particles.

In the single fluorophore regime, reliable stoichiometric assignment is possible by using labeling at a defined ratio. The reliability then depends only on the inherent intensity fluctuations of the dye molecule used. In this regime of very low fluorescence intensities, the stochastic nature of photon emission leads to statistical distributions of the actual detected fluorescence, which can be characterized and taken into account for assignment of local stoichiometries. Using the approach of single molecule counting, the number of fluorescence labeled ligands bound to individual membrane anchored receptor molecules could be determined, allowing for digital analyte quantitation on a molecular level [36].

3.2. Co-localization of different molecules

Two different strategies have been employed to study colocalization of different molecules: single pair fluorescence resonance energy transfer (FRET) [37] and dual wavelength imaging [38]. FRET between donor and acceptor dyes, also termed Förster energy transfer [39], is, in application to ensembles, a well-established assay for the study of colocalization or clustering of components in, for example, cell membranes [40–42]. Recently, FRET was carried to the ultimate limit of the energy transfer between a single pair (donor–acceptor) of biomolecules (single pair FRET; for a review see Ref. [43]). The strong distance dependence between donor and acceptor molecule on length scales of ~5 nm was utilized to quantify distances on single DNA molecules [37,44], to observe conformational dynamics on single enzymes [45], and to image ligand colocalization on individual receptor molecules [46]. Even first applications to living cells have been demonstrated recently [11].

Dual wavelength imaging, the alternative approach to colocalization, visualizes the positions of two different dye molecules in the same probe. The two images are acquired either consecutively [46] or simultaneously [38,47–49] by imaging the same sample area containing two different dyes using two spectroscopic channels specific for the two fluorophores.

3.3. Orientation

Light absorption of a fluorophore depends on the angle between the polarization of the excitation light and the orientation of the transition dipole of the dye. Using linear polarized light for excitation allows to determine the orientation of a single fluorescent dye by measuring the modulation of the fluorescence signal [50–53]. This is equivalent with measuring the linear dichroism of a single dye. In addition, the polarization of the fluorescence signal emitted from the fluorophore can be determined by introducing a polarizing beam-splitter in the emission path of the microscope [54–56]. This methodology has been applied for determination of the axial rotation of actin filaments sliding along myosin molecules [56], for monitoring conformational changes in single myosin molecules [54], for observing subunit rotation of enzymes [57], and for observation of the rotational diffusion of individual lipids in an artificial lipid membrane [55]. Combination of both polarized excitation and determination of the emission polarization allows for steady state anisotropy measurements on a single molecule [55,58], which opens the possibility to access nanosecond time-scales for probing single molecule reorientation. In addition, determination of the polarization can be performed for two colors simultaneously [17,47]. This allows combined measurements of dye orientation and energy transfer, yielding much deeper insights into molecular reorganizations of large biomolecules.

The basic limitation of this approach is its restriction to the study of the in-plane component of the orientation of a dye molecule. In conventional wide field microscopy, the polarization of the excitation light lies mainly in the focal plane. Attempts to access the full orientation of a molecule are therefore based on methodologies with a high z-component in the polarization, like near field microscopy [59,60] or modified confocal microscopy [61]. From the image pattern, the azimuth and elongation angle of a dye molecule can be calculated.

4. Application to genomics/proteomics

Chip-technology has become the prevalent method for investigation of differential gene expression [62] and proteomics [63]. Its current applicability, however, is restricted by the large amounts of sample required. The development of new platforms for high-throughput identification and characterization of biomolecules at lowest concentrations is one major research goal in biotechnology. Such a device represents the technical environment for a "lab on the chip". Rapid identification and quantification of all bound protein molecules define the required specification of this readout device. Currently, planar waveguide-based excitation allows quantification of protein amounts on chip surfaces down to ~500 molecules per spot of 150 μm diameter [4]. Ultimately, individual molecules will be bound to distinct loci on the chip.

The tremendous sensitivity of single molecule microscopy enables the investigation of samples containing only trace amounts of proteins. For estimation, we will describe briefly the binding of proteins in solution to a chip surface coated with a high density of specific antibodies. Using first order binding kinetics, one obtains for the surface density of bound proteins, $\rho_{Ab\text{-}P}$

$$\rho_{Ab\text{-}P} = \frac{Ab + P + VK_D N_A}{2A} - \sqrt{\left(\frac{Ab + P + VK_D N_A}{2A}\right)^2 - \frac{PAb}{A^2}} \quad (1)$$

with Ab, the number of immobilized antibodies, P the number of protein molecules in solution, A the area of the antibody spot on the chip, V the volume of the protein solution, K_D the dissociation constant, and N_A the Avogadro-number. Application of a sample containing only 300 molecules of a specific protein onto a protein chip will result in ~75 protein molecules bound to a distinct capture area of $\sim 10^4$ μm^2.

To ensure optimum binding conditions, local densities of ~1 antibody per 100 nm^2 are assumed, yielding a final amount of $\sim 10^6$ capture antibodies per spot. Fig. 3 shows the theoretical calibration curve for an overall sample volume of 1 nl, a capture antibody density of 1/100 nm^2, a K_D of 1 nM, and a spot size of 10 μm (solid line) and 100 μm (dashed line). The spot size can be used to adjust the linear region for optimum quantification. The overall binding efficiency covers a range of six orders of

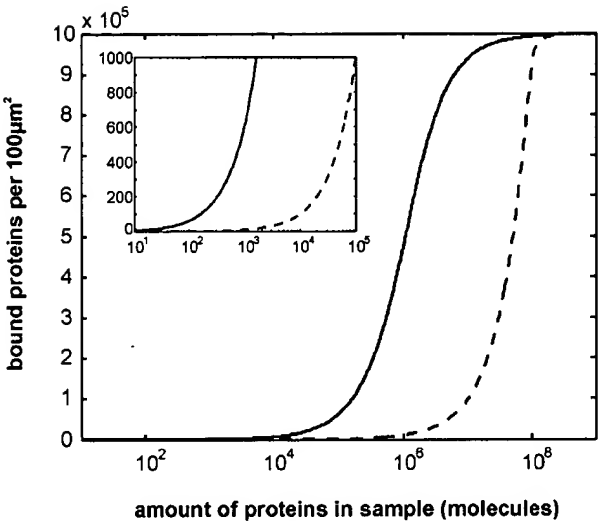

Fig. 3. Figure of merit for protein profiling. The binding curve shows the number of protein molecules immobilized on the capture area, as a function of the amount contained in the sample. The solid (dashed) line was calculated for a spot size of 10 μm (100 μm), using Eq. (1). For both curves, an overall sample volume of 1 nl, a capture antibody density of 1/100 nm^2 and a K_D of 1 n*M* were assumed. At low concentrations, the sensitivity of the "Nanoreader" is inevitable for quantification (insert).

magnitude, which fits to the dynamic range of the "Nanoreader".

Single molecule microscopy requires new strategies for image analysis. Firstly, low signal levels have to be identified and quantified over a background of random noise by implementing new fitting algorithms. Secondly, the sheer amount of data produced in high resolution imaging demands for digital pre-processing to enable rapid data analysis.

The increased information content of single molecule measurements compared to experiments on ensembles of molecules allows to design novel types of assays. Additional screening parameters come into reach, like receptor occupancies, colocalization of different ligands on one receptor, or even details like receptor–ligand-orientations. The full impact of this new information for drug-screening—but also medical diagnostics—has yet to be proven. Single molecule screening techniques have shown their feasibility for routine measurements in a scientific environment; for their general application, however, easy-to-use systems still have to be developed. In combination with novel software algorithms, ultrasensitive imaging techniques are foreseen to become standard equipment for laboratories performing biological diagnostics.

Acknowledgements

We would like to thank Mark Christenson (Roper Scientific) for continuous technical help and Amersham Pharmacia Biotech for general support. This work was funded by the Austrian Research Funds, grant P15053, and the State of Upper Austria.

References

[1] R.L. Strausberg, J. Pathol. 195 (2001) 31.
[2] B. Schweitzer, S. Roberts, B. Grimwade, W. Shao, M. Wang, Q. Fu, Q. Shu, I. Laroche, Z. Zhou, V.T. Tchernev, J. Christiansen, M. Velleca, S.F. Kingsmore, Nat. Biotechnol. 20 (2002) 359.
[3] Z. Zhang, S. Krylov, E.A. Arriaga, R. Polakowski, N.J. Dovichi, Anal. Chem. 72 (2000) 318.
[4] M. Pawlak, E. Schick, M.A. Bopp, M.J. Schneider, P. Oroszlan, M. Ehrat, Proteomics 2 (2002) 383.
[5] W.E. Moerner, L. Kador, Phys. Rev. Lett. 62 (1989) 2535.
[6] W.E. Moerner, M. Orrit, Science 283 (1999) 1670.
[7] E.B. Shera, N.K. Seitzinger, L.M. Davis, R.A. Keller, S.A. Soper, Chem. Phys. Lett. 174 (1990) 553.
[8] I. Sase, H. Miyata, J.E. Corrie, J.S. Craik, K. Kinosita Jr., Biophys. J. 69 (1995) 323.
[9] T. Funatsu, Y. Harada, M. Tokunaga, K. Saito, T. Yanagida, Nature 374 (1995) 555.
[10] T. Schmidt, G.J. Schutz, W. Baumgartner, H.J. Gruber, H. Schindler, Proc. Natl. Acad. Sci. USA 93 (1996) 2926.
[11] Y. Sako, S. Minoghchi, T. Yanagida, Nat. Cell. Biol. 2 (2000) 168.
[12] G.J. Schutz, G. Kada, V.P. Pastushenko, H. Schindler, EMBO J. 19 (2000) 892.
[13] G.J. Schutz, V.P. Pastushenko, H.J. Gruber, H.-G. Knaus, B. Pragl, H. Schindler, Single Mol. 1 (2000) 25.
[14] S. Nie, D.T. Chiu, R.N. Zare, Science 266 (1994) 1018.
[15] E. Bismuto, E. Gratton, D.C. Lamb, Biophys. J. 81 (2001) 3510.
[16] S. Wennmalm, L. Edman, R. Rigler, Proc. Natl. Acad. Sci. USA 94 (1997) 10641.
[17] C. Eggeling, S. Berger, L. Brand, J.R. Fries, J. Schaffer, A. Volkmer, C.A. Seidel, J. Biotechnol. 86 (2001) 163.
[18] U. Haupts, S. Maiti, P. Schwille, W.W. Webb, Proc. Natl. Acad. Sci. USA 95 (1998) 13573.
[19] J. Korlach, P. Schwille, W.W. Webb, G.W. Feigenson, Proc. Natl. Acad. Sci. USA 96 (1999) 8461.
[20] O. Krichevski, G. Bonnet, Rep. Prog. Phys. 65 (2002) 251.
[21] M. Auer, Drug Discov. Today 6 (2001) 935.

[22] A. Van Orden, R.A. Keller, W.P. Ambrose, Anal. Chem. 72 (2000) 37.
[23] M. Minsky, Scanning 10 (1988) 128.
[24] J.B. Pawley, Handbook of Biological Confocal Microscopy, Plenum, New York, 1995.
[25] X.H. Xu, E.S. Yeung, Science 275 (1997) 1106.
[26] R.M. Dickson, A.B. Cubitt, R.Y. Tsien, W.E. Moerner, Nature 388 (1997) 355.
[27] R.M. Dickson, D.J. Norris, Y.L. Tzeng, W.E. Moerner, Science 274 (1996) 966.
[28] T. Schmidt, G.J. Schutz, W. Baumgartner, H.J. Gruber, H. Schindler, J. Phys. Chem. 99 (1995) 17662.
[29] C. Eggeling, J. Widengren, R. Rigler, C.A. Seidel, Anal. Chem. 70 (1998) 2651.
[30] S. Chandrasekar, Rev. Mod. Phys. 15 (1943) 1.
[31] E.H. Hellen, D. Axelrod, Rev. Sci. Instrum. 61 (1990) 3722.
[32] G.J. Schutz, M. Sonnleitner, P. Hinterdorfer, H. Schindler, Mol. Membr. Biol. 17 (2000) 17.
[33] G.J. Schutz, H. Schindler, T. Schmidt, Biophys. J. 73 (1997) 1073.
[34] P.M. Goodwin, M.E. Johnson, J.C. Martin, W.P. Ambrose, B.L. Marrone, J.H. Jett, R.A. Keller, Nucl. Acids Res. 21 (1993) 803.
[35] D. Gross, W.W. Webb, Biophys. J. 49 (1986) 901.
[36] T. Schmidt, G.J. Schutz, H.J. Gruber, H. Schindler, Anal. Chem. 68 (1996) 4397.
[37] T. Ha, T. Enderle, D.F. Ogletree, D.S. Chemla, P.R. Selvin, S. Weiss, Proc. Natl. Acad. Sci. USA 93 (1996) 6264.
[38] T. Ha, T. Enderle, D.S. Chemla, S. Weiss, IEEE J. Select. Top. Q.E. 2 (1996) 1.
[39] T. Förster, Ann. Physik 6 (1948) 55.
[40] A.K. Kenworthy, M. Edidin, J. Cell. Biol. 142 (1998) 69.
[41] D.L. Taylor, Y.-L. Wang, Fluorescence Microscopy of Living Cells in Culture Part B, Academic Press, San Diego, 1989.
[42] N.P. Mahajan, K. Linder, G. Berry, G.W. Gordon, R. Heim, B. Herman, Nat. Biotechnol. 16 (1998) 547.
[43] T. Ha, Methods 25 (2001) 78.
[44] A.A. Deniz, M. Dahan, J.R. Grunwell, T. Ha, A.E. Faulhaber, D.S. Chemla, S. Weiss, P.G. Schultz, Proc. Natl. Acad. Sci. USA 96 (1999) 3670.
[45] T. Ha, A.Y. Ting, J. Liang, W.B. Caldwell, A.A. Deniz, D.S. Chemla, P.G. Schultz, S. Weiss, Proc. Natl. Acad. Sci. USA 96 (1999) 893.
[46] G.J. Schutz, W. Trabesinger, T. Schmidt, Biophys. J. 74 (1998) 2223.
[47] L. Cognet, G.S. Harms, G.A. Blab, P.H. Lommerse, T. Schmidt, Appl. Phys. Lett. 77 (2000) 1.
[48] T. Enderle, T. Ha, D.S. Chemla, S. Weiss, Ultramicroscopy 71 (1998) 303.
[49] K. Saito, M. Tokunaga, A.H. Iwane, T. Yanagida, J. Microsc. 188 (1997) 255.
[50] G.J. Schutz, H. Schindler, T. Schmidt, Opt. Lett. 22 (1997) 651.
[51] A.G.T. Ruiter, J.A. Veerman, M.F. Garcia-Parajo, N.F. van Hulst, J. Phys. Chem. 101 (1997) 7318.
[52] T. Ha, T. Enderle, S. Chemla, R. Selvin, S. Weiss, Phys. Rev. Lett. 77 (1996) 3979.
[53] F. Güttler, J. Sepiol, T. Plakhotnik, H. Mitterdorfer, A. Renn, U.P. Wild, J. Lumin. 56 (1993) 29.
[54] D.M. Warshaw, E. Hayes, D. Gaffney, A.M. Lauzon, J. Wu, G. Kennedy, K. Trybus, S. Lowey, C. Berger, Proc. Natl. Acad. Sci. USA 95 (1998) 8034.
[55] G.S. Harms, M. Sonnleitner, G.J. Schutz, H.J. Gruber, T. Schmidt, Biophys. J. 77 (1999) 2864.
[56] I. Sase, H. Miyata, S. Ishiwata, K. Kinosita Jr., Proc. Natl. Acad. Sci. USA 94 (1997) 5646.
[57] K. Adachi, R. Yasuda, H. Noji, H. Itoh, Y. Harada, M. Yoshida, K. Kinosita Jr., Proc. Natl. Acad. Sci. USA 97 (2000) 7243.
[58] T. Ha, J. Glass, T. Enderle, S. Weiss, Phys. Rev. Lett. 80 (1998) 2093.
[59] J.A. Veerman, M.F. Garcia-Parajo, L. Kuipers, N.F. van Hulst, J. Microsc. 194 (1999) 477.
[60] E. Betzig, R.J. Chichester, Science 262 (1993) 1422.
[61] B. Sick, B. Hecht, L. Novotny, Phys. Rev. Lett. 85 (2000) 4482.
[62] D.J. Lockhart, E.A. Winzeler, Nature 405 (2000) 827.
[63] G. MacBeath, S.L. Schreiber, Science 289 (2000) 1760.

APPENDIX D

"High-throughput scanning with single molecule sensitivity" by Sonnleitner, et al., Proc. SPIE, 5699 (2005):202-210

High-throughput scanning with single-molecule sensitivity

M. Sonnleitner [*a], G. Freudenthaler [a], J. Hesse [b], G.J. Schütz [b]
[a] Center for Biomedical Nanotechnology, Upper Austrian Research GmbH, Scharitzerstr. 6-8, 4020 Linz, Austria
[b] Institute for Biophysics, University of Linz, Altenberger Str. 69, 4040 Linz, Austria

ABSTRACT

We report on the application of a novel fluorescence-microscope based scanning device with single molecule sensitivity to microarray readout. The device is based on a CCD camera operated in time delay and integration (TDI) mode synchronized with the movement of a sample scanning stage, enabling continuous data acquisition. The implementation of a focus hold system keeps the sample in focus during scanning. Results from ultra-sensitive high-resolution microarray readout provide clear evidence for the superiority of the novel detection method over conventional microarray readout systems in particular regarding to sensitivity and dynamic range. Minute sample amount and lacking amplification methods will demand for this ultra-sensitive readout technology in future genomic and proteomic research.

Keywords: Single-molecule detection, high-throughput scanning, autofocus, microarray readout, CytoScout

1. INTRODUCTION

In the early nineties the detection of single fluorescent molecules was for the first time accomplished in condensed matter at low temperatures for the investigation of spectroscopic properties of single dye molecules [1]. During the following decade different techniques in ultra-sensitive fluorescence microscopy at room temperature i.e. polarization microscopy [2, 3], single-molecule imaging, energy transfer [4], lifetime studies were applied to a number of biophysical problems to gain new insight from direct observations of hidden static and dynamic inhomogeneity. The detection of single molecules in living cells [5-7]represents the latest milestone in the application of single molecule detection to biosciences.

In parallel to the advances in ultra-sensitive fluorescence microscopy, a novel striking technology emerged in the field of genetic research and biomedical diagnostics: microarray technology, which during the last years has been applied to various areas of research like tumor classifications [8-10], identification of genes involved in various diseases, cellular responses, or induced responses to external stimuli[11-13], elucidation of biological pathways [14] *et cetera*. It allows to generate data on the expression levels of tens of thousands of genes in a single experiment. A state of the art high-density cDNA microarray contains up to 40.000 spots each with a mean diameter of 150 to 200 µm covering an area of ~10cm^2.

One of the most critical tasks during microarray analysis is the readout process, most commonly based on fluorescence detection. Sensitivity, reproducibility and readout velocity represent three key issues for the readout process. Without any doubt, a scanning technology with single molecule sensitivity and diffraction limited resolution capable of reading out a whole biochip within minutes would be the method of choice for microarray readout. Still, so far such methodology was lacking. Conventional readout systems are based on pixel-wise scanning. With such scanning procedure, reasonable scanning times for 10cm^2 on a minutes time scale are only possible with a pixel resolution of ~5 to 10µm and restricted sensitivity due to limited illumination times.

Here we present a novel scanning mode that allows to read out microarrays with single-molecule sensitivity and diffraction limited resolution in scanning times comparable to times yielded by conventional scanning devices.

To verify the advantages of the technology we applied this readout mode to a state of the art high-density cDNA microarray. The results provide clear evidence for the superiority of the novel technology over conventional systems in particular regarding to sensitivity, dynamic range and recognizing defective spot morphology.

* max.sonnleitner@uar.at; phone 43 732 60 60 79-17; fax 43 732 60 60 79-30

2. METHODOLOGY

2.1 Conventional microarray-readout devices

Conventional microarray-readers for fluorescence detection can be categorized by different operation principles. One category is based on ('confocal') pixel-wise scanning with laser illumination; the second group of scanners takes a series of images ('panels') of adjacent regions of the sample using a white-light lamp for wide-field illumination.

As to confocal scanning, the method is based on scanning a diffraction limited laser focus over the sample; the fluorescence emitted from the sample is imaged onto a point detector. Due to the serial data acquisition the inspection of large sample areas remains a time-consuming task. In particular, in single molecule detection; although the fluorescence of a dye molecule increases linearly with excitation intensity in the low intensity regime, the fluorescence saturates at a certain excitation intensity. Thus, it is not possible to use high illumination intensities to compensate for short illumination times. For common fluorophores this induces minimum pixel dwell times of ~10ms to obtain detectable single molecule signals. For example scanning an area of $1cm^2$ with single molecule sensitivity with a pixel-size of 320nm and the minimum dwell time of 10ms would take 9.9×10^6 seconds (corresponding to 3.8 month!). This implies that diffraction limited confocal scanning with single molecule sensitivity and sub-micron pixel-resolution can not be applied to readout large microarrays within reasonable times. To enable readout of microarrays on a minute timescale with this pixel-wise scanning, conventional readers use pixel-resolutions of 5 to 10 µm.

The second category of scanning systems acquires sequential images in order to cover large areas. In practice this corresponds to a sequence of sample illumination, signal detection, CCD readout and sample movement. The usage of frame-transfer cameras allows to accelerate the measurement by synchronous illumination and readout. In single molecule detection this can only be exploited when using high intensity laser sources instead of white-light lamps to get sufficient excitation intensities. However, proper sample positioning limits the overall readout speed in any sequential recording device. There, inertia of the moving parts requires time-consuming feedback loops for precise stops. A rough estimation for scanning $1cm^2$ (compare[15]) yields about 10 hours scanning time.

2.2 Novel device for ultra-sensitive microarray readout

Here we present a scanning system that avoids overhead times due to both stage positioning and illumination, based on the implementation of synchronized continuous stage-shift and camera readout. For this, the camera is operated in time delay and integration (TDI) mode. In this mode, the CCD chip line shift is synchronized with the object motion, so that charge packets on the CCD pixels always correspond to the same image region as they move across the CCD chip. Charge accumulates and signal strength increases as the pixels approach the readout register. For application of the TDI mode to microscopy, we synchronized image and sample shift using the camera as master triggering the scanning stage upon each line shift. Continuous readout enables the acquisition of images larger than the CCD chip size in line-shift direction, only limited by the storage capacity of the computer. In this readout mode, the scanning speed is only limited by the line-shift speed of the camera. With the device described below, $1cm^2$ can be scanned with single molecule sensitivity within 20 minutes.

2.2.1 Instrument

We developed a high-throughput scanning device with single-molecule sensitivity based on this novel patented readout mode for microscopy [16]. In general, the device comprises laser-illumination, an inverted microscope, a high precision scanning stage, cooled CCD cameras for detection and a novel patented focus hold system.

Fig. 1 shows a detailed illustration of the system. For Illumination we use an Ar-Kr-mixed gas 'whitelight'-laser (Coherent, USA) with distinct laserlines at 457, 476, 488, 514, 520, 568 and 647 nm. In multiline mode the laser provides a mean output power of 2.5W. A polychromatic acousto optical modulator (NEOS technologies, USA) allows to select individual lines or any combination of available laserlines. In addition to the laserline selection, the individual power of the selected lines can be set by adjusting the amplitude of the driving signal applied to the modulator. After a pinhole to separate the different deflection orders of the modulator we yield 50 to 300mW output in the diverse laserlines.

The beam is coupled into the back port of an inverted microscope (Axiovert 200, Zeiss, Germany) and subsequently passes a Powell lens (OZ Optics, USA). This component transforms the circular beamshape into a quasi rectangular, with a Gaussian profile in vertical and a nearly homogenous profile in horizontal direction (for details refer to [17]). A freely adjustable rectangular aperture at the field diaphragm of the illumination pathway enables to generate a

rectangular illumination area at the sample plane. The sharp edges of the illumination area avoid bleaching of adjacent scanned stripes.
The excited fluorescence is collected using a 100x oil immersion objective (Plan Neofluar, NA = 1.45, Zeiss, Germany) and discriminated from excitation by a dichroic mirror (Chroma, USA). A second dichroic splits and images the fluorescence generated by different fluorophores onto cooled CCD detectors (CoolSnap HQ, Roper Scientific, USA).
The small depth of focus of high-NA objectives in the µm range demands for a procedure to keep the sample in focus during scans of large areas. For this we developed an automatic focus-hold system. A near infrared laser-diode with 10 mW is overlaid with the illumination beam and imaged onto the sample next to the detection area. Upon reflection on the upper glass surface, the beam is re-collimated through the objective. Changes in the distance between the surface of the coverslip and the objective result in changes in the angle of the out-coupled beam, which are detected on a two-segment photodiode (Hamamatsu, Japan). The differential signal was used as input into a PID controller operated in feedback loop; the output of this controller was connected to a piezodriven focusing system (Physik Instrumente, Germany).

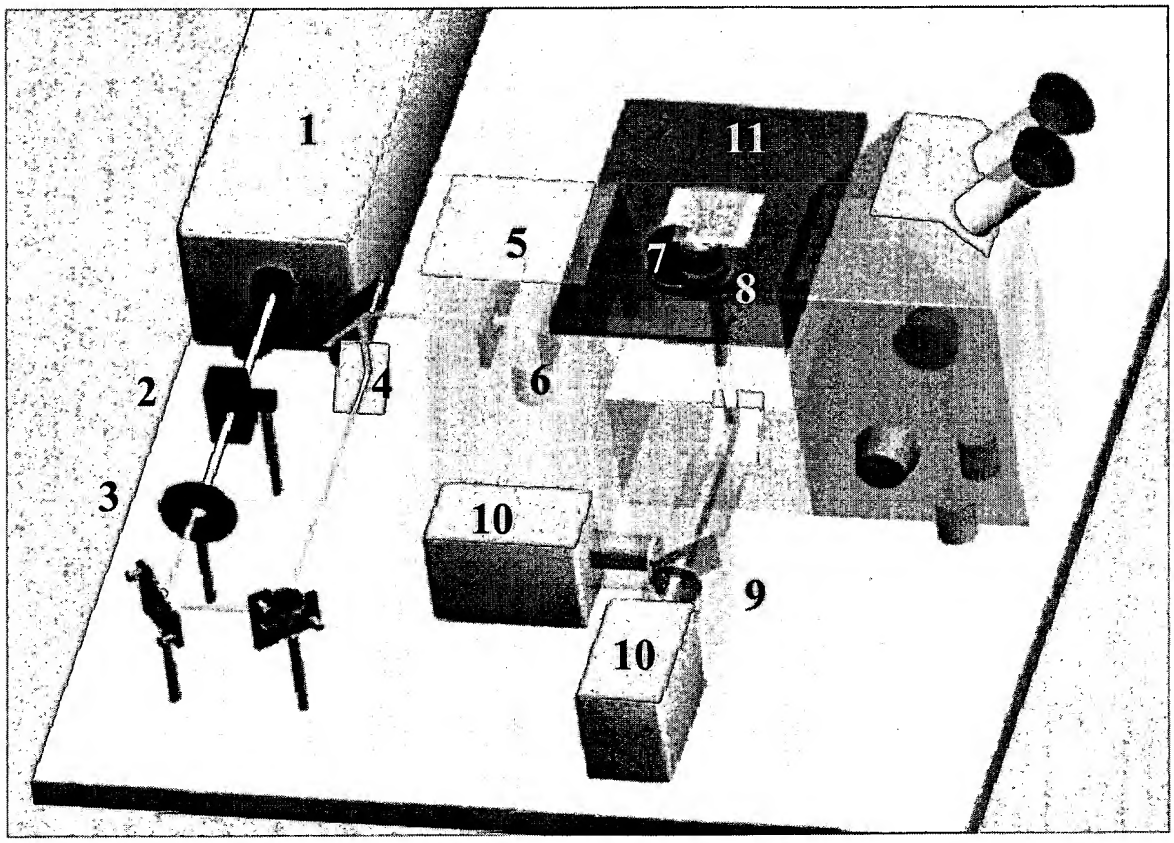

Figure 1: Illustration of the ultra-sensitive readout device: 1...white-light-laser, 2...polychromatic acousto-optical-modulator, 3...pin-hole, 4...beam-lifter, 5...Powell-lens, 6...rectangular-diaphragm, 7...z-piezo, 8...objective, 9...dual-video-adapter, 10...camera, 11...high-precision x/y-stage

3. MEASUREMENTS AND RESULTS

To test the advantages of our ultra-sensitive detection device in microarray readout, we scanned a state of the art high-density cDNA-microarray provided by the group of H. Lehrach (Max Planck Institute for Molecular Genetics, Berlin, Germany). The spotted area containing about 40.000 spots with a mean diameter of ~150µm has a region of 18 x 53mm. Cy3 labeled RNA was hybridized to the spots.

The microarray was scanned in Berlin with a conventional microarray reader by means of pixel-wise scanning with 532nm laser excitation and a pixel-size of 10μm. For ultra-sensitive scanning we applied the CytoScout® as illustrated in Fig. 1 with 514 and 520nm laser-lines for illumination. Using a 100x objective, a camera pixel-size of 6.45 μm and binning 8 gives a pixel-size of 516nm in the image.
The thickness of the microarray glass-slide prevented us from scanning the entire chip in one procedure. Therefore, to compare ultra-sensitive detection with conventional scanning, we choose regions of interest from data collected by the conventional scanner.
The measurements clearly verify the advantages of ultra-sensitive high-resolution CytoScout® readout in sensitivity, resolution and dynamic range.

3.1 Sensitivity

For a comparison in scanning sensitivity we chose a region on the microarray, which contains spots no more observable by the conventional scanner. Fig. 2 shows data collected from such region of interest collected by ultra-sensitive and high-resolution scanning. Data recorded by the conventional device of the corresponding region is illustrated for comparison. To visualize the limits of spot detection in the different systems, the scaling of images was adapted to even notice variations in background. It is evident, that spots no more distinguishable from background by the conventional scanner can be discriminated from background in the ultra-sensitive and high-resolution scan.
For quantification, we investigated seven spots (as indicated). The zoom in of conventional scanner data reveals 3 spots, two of them clearly observable and one hardly distinguishable from background. Ultra-sensitive data was acquired with 0.516μm (compared to 10μm) pixel-size. This implies, that signal collected in one image pixel by the conventional device is spread over 375 pixels of the detector used in the CytoScout®-scanner.
In consequence, local signal variations within a spot on the sub-pixel (10 x 10μm) scale can not be resolved by the conventional scanner. Therefore, if accumulated fluorescence signal within one pixel is smaller than noise, the very pixel will not be distinguishable from background. In contrast, ultra-sensitive high-resolution scanning even allows to detect single-fluorescent molecules [17] and locate the signals with a precision of down to ~50nm [18]. In this case even the smallest signals within a pixel can be discriminated from background noise and by this the signal to noise ratio is clearly improved compared to the conventional device. This is demonstrated in the zoom in of ultra-sensitive data. Background is subtracted from the original image with 0.516μm pixel-size and via software binning the pixel-size is adapted to 10μm equivalent to the pixel size of the conventional scanner. This renders direct comparison of signals possible.
This is shown in Fig. 2C on a logarithmic scale of the integrated pixels along a row. Each of the spots is clearly observable with the ultra-sensitive CytoScout®, while the conventional scanner is not able to distinguish 4 of the spots from background noise. The integrated signal from the top spot collected by the CytoScout® is 25 times higher than the corresponding signal detected by the conventional scanner. The signal to background noise ratio for this spot is improved by a factor of ~10.

3.2 Spot Morphology

The hurdle of reproducibility of results from microarray analysis has still to be taken. One of the major problems lies in the spotting procedure itself. A variety of parameters can influence the spotting results [19]. A 'good' spot is characterized by a circular shape and homogenous distribution of the spotted molecule over the entire spot. 'Bad' spots can have doughnut effects, clumps, scratches or dye separation [20]. Testing procedures for spotting allow to optimize the average spot of a spotting robot. However, on a high density microarray thousands of spots have to be applied and variation in spot morphology is a given fact. In consequence, the morphology of each spot has to be concerned during analysis. For that, spot morphology has to be characterized as precisely as possible. Assuming a conventional scanner with a pixel-size of 10 μm, a spot of 150μm diameter is imaged onto ~150 pixels. Spot inhomogeneities on a smaller lateral scale than 10μm are not resolved. With high-resolution detection and 0.516μm pixel-size, the spot is imaged onto ~65 000 pixels.
Fig. 3 illustrates this unequal ratio of conventional to high-resolution data. The same spot was scanned with a pixel resolution of 10μm with the conventional scanner and for comparison with 0.516μm resolution with the CytoScout®. The high-resolution image of the spot clearly reveals strong spot inhomogeneity, which would restrict this spot from further analysis. The conventional scanner collected a homogenous signal from the spot. In this case the signal would be further analyzed and consequently yield a false-positive result.

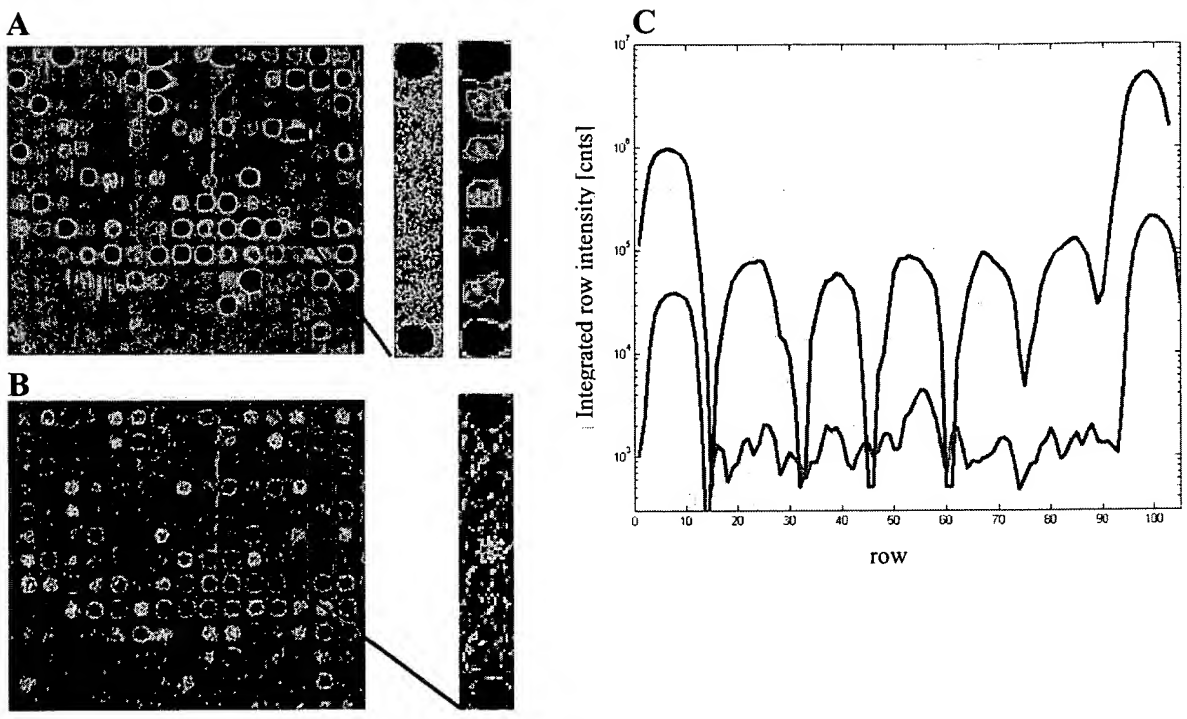

Figure 2: Comparison of a conventional scanner (B) with the CytoScout® (A) in ultra-sensitive detection mode (100x objective, NA=1.45, 516nm pixel size). A substantial fraction of spots not recognizable by the commercial scanner yields clearly detectable signals on the CytoScout®. The details further illustrate this finding. For comparison, signals were software-binned to the pixel-size of the commercial device, and C plotted as cross-section on a logarithmic scale (red line: CytoScout®, green line: conventional scanner).

3.3 Dynamic Range

One essential performance parameter in microarray analysis is the dynamic range of the platform. Low as well as high abundant molecules should be detected within one readout process. The dynamic range of conventional scanners is limited by 16 bit per pixel corresponding to 65536 intensity levels. Assuming spot diameters of ~150 µm and 10 µm pixel-size this corresponds to 175 pixels per spot. For comparison, in high-resolution readout the spot's fluorescence is collected on ~65 000 pixels each with a dynamic range of 12-bit. This results in an increase in saturation threshold by a factor of 25. A maximum increase in saturation threshold of even 20.000 can be achieved by using the CytoScout® system with 16 bit cameras and the smallest available pixel-size of 65 nm.

In Fig. 4 the effect of this difference is demonstrated. A region of data acquired by the conventional scanner is compared to the same region scanned by the ultra-sensitive high-resolution CytoScout®. Three spots (as indicated) appear already saturated when scanned with the conventional device and hence are no more distinguishable by means of their signal levels. In contrast, the increased dynamic range of the CytoScout® allows to readily discriminate the different expression levels of the corresponding RNA (compare Fig. 4C).

Fig. 4 reveals the increase in saturation threshold by high-resolution scanning with impact on the detection of high abundant RNA. On the other hand, the single-molecule-sensitivity of the CytoScout® expands the dynamic range of this detection method towards the analysis of low abundant RNA.

From the given scanning parameters i.e. illumination intensity, exposure time, photo-physical properties of the fluorophore, detection efficiency of the microscope-system, the fluorescence collected from a single fluorophore can be calculated [21]. This enables to retrieve the number of labeled analyte molecules bound within a spot. In Fig. 5 the signal to noise ratio is plotted versus the number of fluorophores per spot estimated for both scanning devices. Continuous

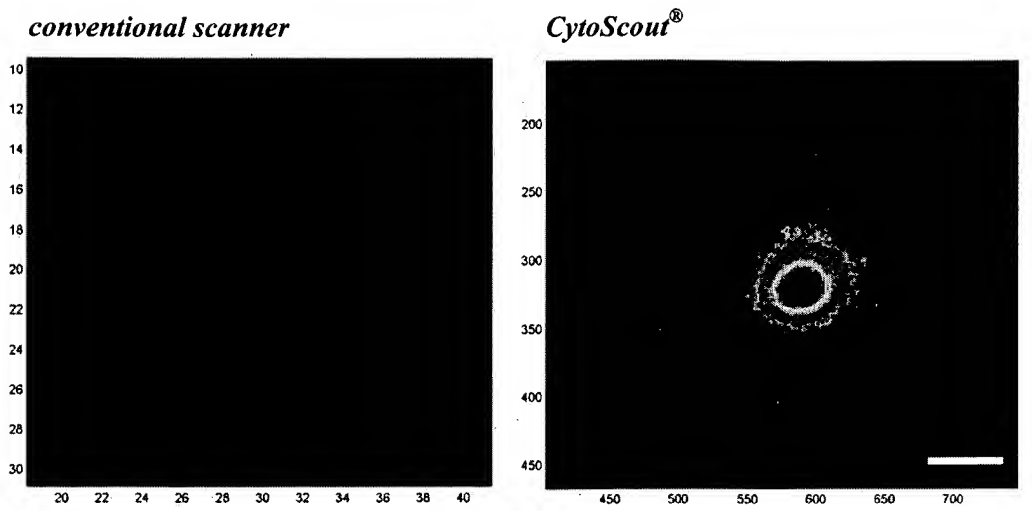

Figure 3: The same spot scanned with the conventional scanner (left) and with the CytoScout® (right, bar: 25μm). The pixelsize of 10μm of the commercial scanner does not allow to resolve defects in the spot-morphology as illustrated in the images. This will lead to false-positive results. CytoScout® with a pixel-size of 516nm (down to 65 nm possible) resolves even the smallest defects and thus prevents false/positives.

lines correspond to the signal to noise ratio for ensemble measurements, with their curves progression reflecting the noise contributions in ensemble studies. For a reasonable signal to noise ratio of 10 the superiority of ultra-sensitive detection already becomes evident. However, if we in addition account for the capability of the CytoScout® to count single molecules within a spot (dotted line) the ensemble noise does not contribute anymore as reflected by the linearity of the dotted line.

Taken together, the combination of single-molecule sensitivity and increased saturation threshold by high pixel-resolution expands the dynamic range of the CytoScout to six orders of magnitude compared to three orders of magnitude dynamic range of the conventional device.

4. SUMMARY AND OUTLOOK

In this paper we apply high-throughput scanning with single-molecule sensitivity to microarray readout and verify the superiority of this novel high-throughput readout technology over conventional scanning methods. By this, we bring together two core technologies from biophysics and genetics and open up new perspectives in biomedical research and diagnostics. Although, for nucleic acid detection, the problem of limited sample size can be bypassed using PCR- based amplification. (however, often leading to complications due to cross-contamination of sample material, and distorted statistical outputs), for the analysis of proteins direct amplification methods are still lacking. From this line of argumentation, an ultra-sensitive detection device as described here is mandatory for any future genomics and proteomics platform.

ACKNOWLEDGEMENTS

The authors would like to thank H. Lehrach (Max Planck Institute for Molecular Genetics, Berlin, Germany) for providing the cDNA microarray together with the data collected by the conventional scanning device.

The study was supported by the GEN-AU program of the Austrian Federal Ministry of education, Science and Culture, and by the state of Upper Austria.

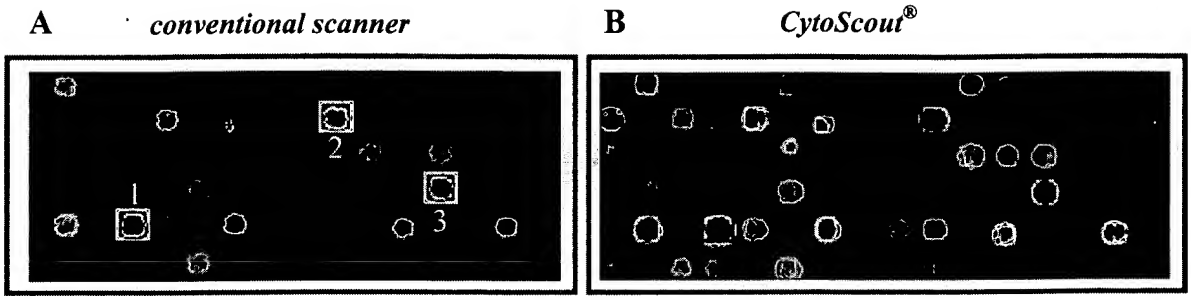

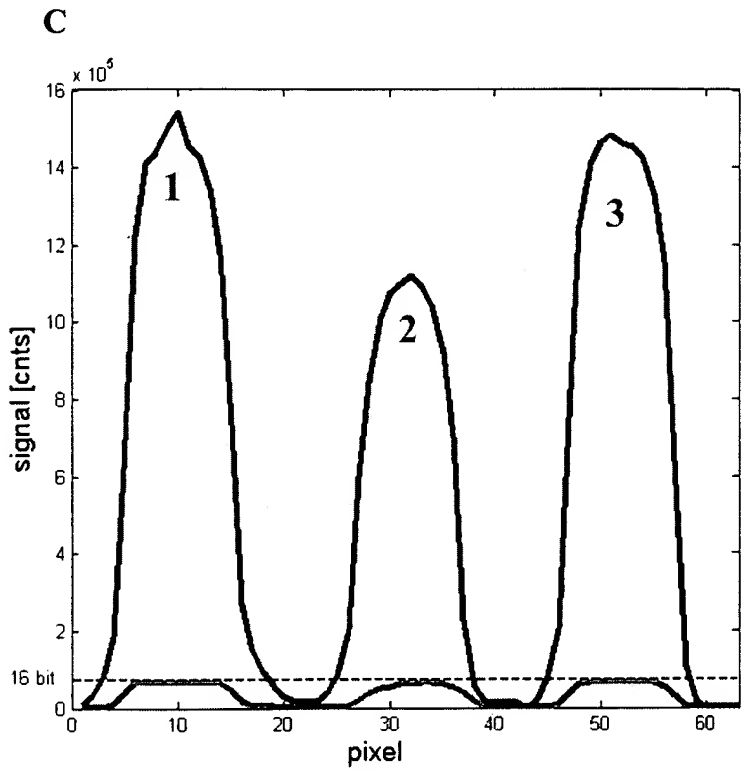

Figure 4: Due to higher resolution imaging, a single pixel on a commercial scanner corresponds to ~400 pixels (each pixel with 12 bit) on the CytoScout®. This increases the signal saturation threshold of the CytoScout® by a factor of 25 compared to commercial devices. 3 high intensity spots have been selected for illustration (A and B show scans of a commercial device and the CytoScout®, respectively). C shows cross-sections through the selected spots. While the signals reach saturation on the commercial device (green line), they can readily be quantified on the CytoScout® (red line).

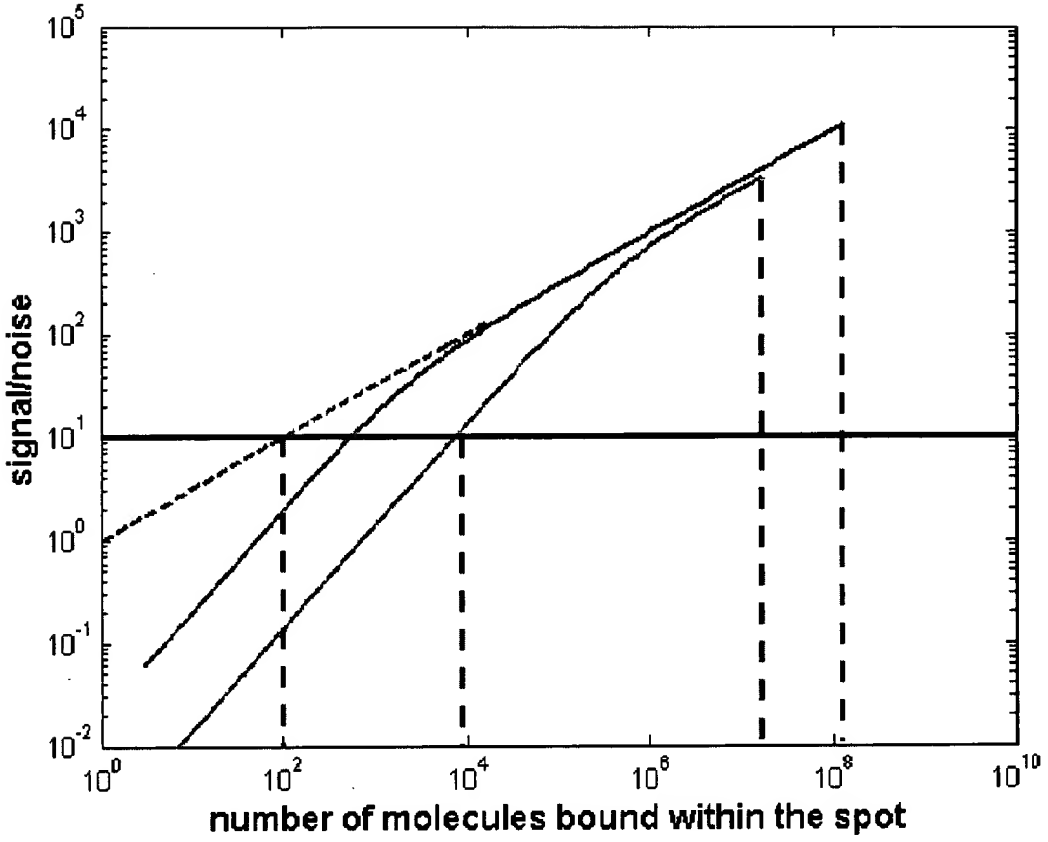

Figure 5: Illustration of the increase in dynamic range of the CytoScout® (red lines) compared to a conventional scanner (green line). Continuous lines show the signal to noise ratio for ensemble measurements accounting for noise contributions. The dotted red line reflects the capability of the CytoScout® to detect and count single molecules without ensemble noise. Both the ability to detect single-molecules and the high pixel-resolution contribute to the improvement in dynamic range.

REFERENCES

1. W. E. Moerner, L. Kador. *Optical detection and spectroscopy of single molecules in a solid.* Physical Review Letters; 62: 2535-2538, 1989.
2. L. Cognet, G. S. Harms, G. A. Blab, P. H. Lommerse, T. Schmidt. *Simultaneous dual-color and dual-polarization imaging of single molecules.* Appl. Phys. Lett.; 77: 1-3, 2000.
3. G. S. Harms, M. Sonnleitner, G. J. Schütz, H. J. Gruber, T. Schmidt. *Single-molecule anisotropy imaging.* Biophys J; 77: 2864-2870., 1999.
4. T. Ha, T. Enderle, D. F. Ogletree, D. S. Chemla, P. R. Selvin, S. Weiss. *Probing the interaction between two single molecules: fluorescence resonance energy transfer between a single donor and a single acceptor.* Proc Natl Acad Sci U S A; 93: 6264-6268., 1996.
5. Y. Sako, S. Minoghchi, T. Yanagida. *Single-molecule imaging of EGFR signalling on the surface of living cells.* Nat Cell Biol; 2: 168-172., 2000.

6. G. J. Schutz, V. P. Pastushenko, H. J. Gruber, H.-G. Knaus, B. Pragl, H. Schindler. *3D Imaging of Individual Ion Channels in Live Cells at 40nm Resolution.* Single Mol.; 1: 25-31, 2000.
7. G. J. Schutz, G. Kada, V. P. Pastushenko, H. Schindler. *Properties of lipid microdomains in a muscle cell membrane visualized by single molecule microscopy.* Embo J; 19: 892-901., 2000.
8. D. G. Beer, S. L. Kardia, C. C. Huang, T. J. Giordano, A. M. Levin, D. E. Misek, L. Lin, G. Chen, T. G. Gharib, D. G. Thomas, M. L. Lizyness, R. Kuick, S. Hayasaka, J. M. Taylor, M. D. Iannettoni, M. B. Orringer, S. Hanash. *Gene-expression profiles predict survival of patients with lung adenocarcinoma.* Nat Med; 8: 816–824, 2002.
9. T. O. Nielsen, R. B. West, S. C. Linn, O. Alter, M. A. Knowling, J. X. O'Connell, S. Zhu, M. Fero, G. Sherlock, J. R. Pollack, P. O. Brown, D. Botstein, M. van de Rijn. *Molecular characterisation of soft tissue tumours: a gene expression study.* Lancet; 359: 1301–1307, 2002.
10. L. J. van't Veer, H. Dai, M. J. van de Vijver, Y. D. He, A. A. Hart, M. Mao, H. L. Peterse, K. van der Kooy, M. J. Marton, A. T. Witteveen, G. J. Schreiber, R. M. Kerkhoven, C. Roberts, P. S. Linsley, R. Bernards, S. H. Friend. *Gene expression profiling predicts clinical outcome of breast cancer.* Nature; 415: 530–536, 2002.
11. M. J. McDonald, M. Rosbash. *Microarray analysis and organization of circadian gene expression in Drosophila.* Cell; 107: 567–578, 2001.
12. F. A. Middleton, K. Mirnics, J. N. Pierri, D. A. Lewis, P. Levitt. *Gene expression profiling reveals alterations of specific metabolic pathways in schizophrenia.* J Neurosci; 22: 2718–2729, 2002.
13. R. Ohki, K. Yamamoto, H. Mano, R. T. Lee, U. Ikeda, K. Shimada. *Identification of mechanically induced genes in human monocytic cells by DNA microarrays.* J Hypertens; 20: 685–691, 2002.
14. H. Yoshimoto, K. Saltsman, A. P. Gasch, H. X. Li, N. Ogawa, D. Botstein, P. O. Brown, M. S. Cyert. *Genome-wide analysis of gene expression regulated by the calcineurin/Crz1p signaling pathway in Saccharomycescerevisiae.* J Biol Chem; 277: 31079–31088, 2002.
15. J. Hesse, M. Sonnleitner, G. J. Schutz. *Ultra-sensitive fluorescence reader for bioanalysis.* Curr Pharm Biotechnol; 5: 309-319, 2004.
16. H. Schindler. *PCT/AT99/00257.* international patent, 2000.
17. J. Hesse, M. Sonnleitner, A. Sonnleitner, G. Freudenthaler, J. Jacak, O. Höglinger, H. Schindler, G. Schutz. *Single molecule reader for high-throughput bioanalysis.* Anal Chem; 76: 5960-5964, 2004.
18. T. Schmidt, G. J. Schutz, W. Baumgartner, H. J. Gruber, H. Schindler. *Imaging of single molecule diffusion.* Proc Natl Acad Sci U S A; 93: 2926-2929., 1996.
19. D. S. Rickman, C. J. Herbert, L. P. Aggerbeck. *Optimizing spotting solutions for increased reproducibility of cDNA microarrays.* Nucleic Acids Res; 31: e109, 2003.
20. C. S. Brown, P. C. Goodwin, P. K. Sorger. *Image metrics in the statistical analysis of DNA microarray data.* Proc Natl Acad Sci U S A; 98: 8944-8949, 2001.
21. T. Schmidt, G. J. Schutz, H. J. Gruber, H. Schindler. *Local stoichiometries determined by counting individual molecules.* Anal Chem; 68: 4397-4401, 1996.